THE MECHANICAL PROPERTIES OF STEELS STRENGTHENED BY INTERPHASE PRECIPITATION.

J.P.BENSON

ACKNOWLEDGEMENTS.

This research was carried out between October 1976 and September 1978 whilst the author was an SRC supported post-doctoral research assistant in the Department of Metallurgy and Materials Science of the University of Cambridge.

The provision of laboratory facilities by Professor R.W.K.Honeycombe is gratefully acknowledged. I am grateful to Mr. E.C.F.G.Cole, Mr. J.R.Leader and Mr. S.D.Charter for their assistance with the experimental work. Thanks are also due to Dr. D.V.Edmonds, Mr. H.K.D.H.Bhadeshia and other members of the Alloy Steels Research Group for helpful discussions.

J.P.Benson

Cambridge, September 1978.

CONTENTS.

CHAPTER ONE.
INTRODUCTION.

In recent years a considerable amount of work has been carried out with a view to characterising and understanding the microstructures that are formed by transformation of austenite to ferrite by an "interphase precipitation" mechanism and the resulting mechanical properties. The work reported here is a continuation of reference 1.

In chapter two new evidence is presented concerning the impact properties of steels strengthened by interphase precipitation, and the relationship of the cleavage crack path to the microstructure. It is concluded that the main reason for the low toughness of these materials is the large precipitation hardening contribution to the yield strength, there being little modification of the cleavage crack path due to the non-random carbide dispersion.

Chapter three contains further analysis of the results for fatigue in a $\frac{1}{2}$Cr-$\frac{1}{2}$Mo-$\frac{1}{4}$V steel presented in reference 1, together with information on the S-N behaviour of this material and on specimen thickness and load ratio effects in the intermediate fatigue crack growth rate range. It is shown that the exponent 'm' in the Paris Law decreases with increasing yield strength and toughness. There is a slight decrease in 'm' at each load ratio when the specimen thickness is reduced, but this could not be explained by arguments of crack closure, general yield or the onset of plane stress deformation. It is shown that there is a linear relationship between m and logC for fatigue crack growth in the intermediate growth rate range over a wide range of yield strengths, thicknesses and load ratios. There

is some evidence of conflicting requirements for resistance to fatigue crack initiation and to fatigue crack growth in steels.

Chapter four presents results for the effects of grain size and yield strength on the threshold for fatigue in an Fe-Ti-C steel. The threshold value at R=0 is decreased by increasing the yield strength or reducing the ferrite grain size. There is a smaller load ratio effect at higher yield strength levels. The effects of yield strength and load ratio are consistent with a model based on hydrogen embrittlement, but the grain size effect is not fully understood.

Temper embrittlement due to phosphorous and antimony has been investigated, and the results are presented in chapter five. It is shown that the isothermally transformed ferritic microstructures are less susceptible to temper embrittlement than quenched and tempered microstructures in the same material. This may be a reflection of the poor transgranular cleavage properties of the ferritic microstructures.

Chapter six contains a concluding discussion of the mechanical properties of steels strengthened by interphase precipitation and an assessment of their usefulness as commercial materials. Some suggestions are made for further areas to be investigated.

CHAPTER TWO.

CLEAVAGE OF FERRITE CONTAINING NON-RANDOM CARBIDE DISPERSIONS.

Introduction.

Transformation from austenite to ferrite in various alloy steels results in a non-random carbide dispersion. The carbides are arranged in sheets which mark the successive positions of the advancing $\gamma-\alpha$ boundary, and this has been called "interphase precipitation" (2). The mechanisms of the reaction are now understood in considerable detail, and there is much evidence to suggest that the plane of the precipitate sheets is $\{110\}_\alpha$ (3). For carbides of the VC type the Baker-Nutting orientation relationship is found between the carbide and the ferrite matrix, only one of the three possible variants being found in each area (2,4). The individual carbides are platelets on $\{100\}_\alpha$, but the carbides are arranged in sheets which are $\{110\}_\alpha$ (figure 2.1).

It is apparent that these microstructures can have low toughness at high strength levels (5,6). The results of an initial fractographic investigation of possible reasons for this have been published (7), and this chapter presents the results of further mechanical and fractographic investigations.

It is not possible to devise an experiment to produce comparable random and non-random carbide dispersions in the same alloy, and so any effects due to a non-random dispersion must be inferred indirectly. The carbide dispersion can have a number of effects on the cleavage process. It raises the macroscopic yield stress of the material by impeding dislocation motion, and the impact transition temperature will increase with increasing yield stress. Prolonged

ageing of the interphase precipitate dispersion removes the initial sheet structure and produces a more random dispersion (8,9). It is therefore possible to examine the effect on impact transition temperatures of reducing the non-random character of the dispersion.

Any effects due to the non-random dispersion can also result in a change in the path of a cleavage crack through the microstructure. If the carbide dispersion has no effect then cleavage at -196°C will be on $\{100\}_\alpha$, with no particular $\{100\}_\alpha$ preferred. Secondary cracking will occur on the other $\{100\}_\alpha$ planes. For room temperature fracture there may be a slight tendency to fracture on $\{110\}_\alpha$ (10). The interphase dispersion of VC contains platelets on $(100)_\alpha$, as compared with $\{100\}_\alpha$ for a random dispersion. This may lower the cleavage fracture stress on this particular plane, resulting in an increase in impact transition temperature and a preference for cleavage fracture on this specific plane. The interphase precipitate sheets can lie on $(110)_\alpha$. There may be a tendency to encourage $\{110\}_\alpha$ fracture at room temperature on this specific $(110)_\alpha$.

This chapter presents the results of a number of parallel mechanical, fractographic and electron microscope investigations in vanadium steels, and in an Fe-Cu alloy :

1. characterisation of the effect of yield stress and precipitate volume fraction on the impact transition temperature for interphase precipitation dispersions.

2. investigation of the effect of ageing of interphase precipitation, and so producing a more random carbide dispersion, on the yield stress and impact transition

temperature.

3. comparison of the mechanical properties of an Fe-Cu alloy after either isothermal transformation from austenite to ferrite or ageing of solution treated ferrite.

4. scanning electron microscopy of etched fracture surfaces of coarse carbide dispersions after cleavage at -196°C and room temperature to obtain information on the path of the cleavage crack through the microstructure.

5. optical microscopy of the path of cleavage cracks at -196°C and room temperature through a microstructure containing both interphase precipitation and a Widmanstatten precipitate of VC, the three habits of which permit trace analysis of the crack path.

6. transmission electron microscopy to determine the trace of the sheets of interphase precipitation after isothermal transformation.

7. transmission electron microscopy of iron plated fracture surfaces to examine the fine scale crystallography of cleavage in these materials.

Experimental details.

The alloy compositions are given in Table 2.1. The ingots were sectioned, hot rolled and swaged to give rod for the mechanical tests. Oversize specimen blanks were heat treated in tube furnaces with an argon atmosphere and in salt baths, and then subsequently machined to the required dimensions. Hounsfield no.11 specimens were used for the tensile tests. Impact specimens were tested using a Hounsfield balanced impact machine which was adapted for in situ heating and cooling of specimens to the testing temperature.

Two specimen designs were used. For F1,F2,F3 specimens were 6mm. diameter with a 1.2mm. notch depth, and for A1 specimens were 5mm. diameter with a 1.35mm. notch depth. The notch sharpness was constant for F1,F2,F3 and for A1, although different for the two series of tests. A 50% cleavage fracture criterion was used for the impact transition temperature. The use of such small specimens was considered justified because it has been shown that changes in impact transition temperature, as opposed to absolute impact transition temperatures, are comparable for small size specimens and full size Charpy specimens (11).

Transmission electron microscope specimens of some fracture surfaces were prepared. A layer of iron several mm. thick was electroplated onto the fracture surface using an acidic aqueous solution of 500g. $FeCl_2$ + 5g. $MnCl_2$ per litre at 93°C and a current density of 2000 amp./m^2. Slices 0.25mm. thick were then cut from the specimen to include the fracture surface. These slices were ground to 0.05mm. and then discs of 3mm. diameter cut out such that the fracture surface was across the centre of the disc. The discs were then jet polished in 5% perchloric acid in 2-butoxyethanol at -20°C and 85V until a small perforation was obtained, this perforation being enlarged by either continued electropolishing or by ion beam thinning until it crossed the fracture surface. Locating the relevant regions in the electron microscope is difficult, and it is helpful to first examine the foil on an optical microscope, noting the shape of the perforation and the path of the fracture.

The iron plating solution is acidic and it may be

beneficial to evaporate iron onto the fracture surface before electroplating to eliminate the possibility of the plating solution attacking the fracture surface.

Experimental results.

1. The effect of yield stress and precipitate volume fraction on the impact transition temperature.

Alloys F1,F2 and F3 were used in this part of the investigation. Isothermal TTT curves were determined for each alloy to identify the temperature range over which complete transformation from austenite to ferrite was obtained. Specimens were austenitised and then isothermally transformed at a series of temperatures (700-790°C for F1, 660-790°C for F2, 670-790°C for F3). This resulted in a range of yield strengths for each alloy, and the three alloys also differ in their precipitate volume fraction. The results are given as a plot of yield strength against impact transition temperature in figure 2.2. It can be seen that all the results lie in the same scatter band, implying that the yield strength is far more significant than the precipitate volume fraction in determining the impact transition temperature. Regression analysis of the data shows that the impact transition temperature is raised by 0.54°C for each 1MPa increase in yield stress.

2. The effect of ageing on the yield stress and the impact transition temperature.

Alloy A1 was used. It has been shown that ageing a dispersion of interphase precipitated vanadium carbide results in a progressive randomising of the precipitate

dispersion until eventually the original distribution in sheets is removed (8,9). The procedure of the previous section was used to produce as wide as possible a range of yield strengths by isothermal transformation in the range 660-790°C, and then the associated impact transition temperatures were determined. The impact transition temperatures in this section are markedly different to those for alloys F1 to F3 because of the different specimen design, but the rate of change of impact transition temperature with yield stress is comparable. Further specimens were isothermally transformed at 660°C and then aged for 15, 25 or 40 minutes at 790°C, 20, 40 or 90 minutes at 750°C or 30, 60 or 120 minutes at 700°C. The resulting yield stresses and impact transition temperatures were determined. The results are shown in figure 2.3. At a given yield stress, the impact transition temperature is increased by almost 100°C by ageing the precipitate dispersion. Regression analysis of the data shows that the increase of impact transition temperature with yield stress is 0.64°C/MPa in the unaged, as isothermally transformed condition and 0.66°C/MPa in the aged condition. These values are very similar to the value of 0.54°C/MPa found for alloys F1-F3.

3. Comparison of the mechanical properties resulting from random and non-random dispersions, using an Fe-Cu model system.

It is not possible to produce comparable random and non-random dispersions of carbide in ferrite, but an Fe-Cu alloy with copper precipitates provides a simple analogue. Unlike the carbide precipitates, the copper precipitates are softer than the matrix, but elastic modulus hardening

gives a significant contribution to the yield strength (12). The strain energy per unit length of a dislocation depends on the shear modulus, so that if the shear modulus of the precipitate is less than that of the matrix it will be energetically favourable for the dislocations to thread through the precipitates, thereby strengthening the alloy by inhibiting dislocation motion. Simensen (13) showed that isothermal transformation from γ to α in certain Fe-Cu systems resulted in interphase precipitation of copper, although his implication that this is the major precipitation mechanism in these alloys is probably misleading. Several workers have studied the precipitation of copper from supersaturated ferrite (14-17) to show that there is a definite hardening reaction on ageing. Initially copper clusters are formed in the ferrite matrix, then f.c.c. copper rich precipitates are formed, these being spherical and randomly distributed, except at longer ageing times and at higher temperatures when they become rod-shaped.

The objective of this work was to produce comparable random and non-random copper dispersions in ferrite and then to compare their tensile and impact properties. The results are summarised in Table 2.2. The temperatures for heat treatment were selected as follows :

1050°C to ensure complete austenitisation without excessive grain growth

700°C, 725°C to give transformation to ferrite at temperatures which earlier work (13) suggested would give interphase precipitation without interference from the massive reaction

840°C for re-solution of copper in ferrite in the single

Table 2.1 Composition (weight %) of the alloys tested.

	V	C	Mn	Al	Ni	Cu
F1	1.03	0.19	0.03	-	-	-
F2	0.74	0.11	0.03	-	-	-
F3	0.49	0.03	0.03	-	-	-
A1	1.15	0.22	-	-	-	-
A2	0.96	0.21	-	0.97	-	-
E	0.54	0.14	-	-	-	-
J1	-	-	-	-	1.0	1.75

Table 2.2 Tensile and impact properties of the Fe-Cu alloy.

		σ_y (MPa)	σ_u	ITT (°C)
I.	15/1050 + 2/700AC	376	463	-63
II.	15/1050 + 2/720AC	365	460	-73
III.	15/1050 + 2/720AC + 1hr/840WQ + 24hr/600AC	303	371	-13
IV.	15/1050 + 2/720AC + 1hr/840WQ + 48hr/600AC	287	362	-18

phase region of the equilibrium diagram (figure 2.4)

600°C to give significant hardening in 48 hours

These results do not permit any conclusions to be made because, firstly, electron microscopy revealed that isothermal transformation under these conditions did not produce more than 10% interphase precipitation, and, secondly, the precipitation hardening contribution to the yield stress was relatively small, so that the resulting changes in the impact transition temperature are also small. The low percentage of transformation by interphase precipitation is probably due to the intrusion of a massive reaction which results in ferrite supersaturated with respect to copper, this copper precipitating on subsequent air cooling.

In principle it is possible to use this approach to give comparable random and non-random dispersions of copper in ferrite. Further work is required to elucidate the optimum alloy and heat treatments. It may be possible to use the massive reaction and subsequent precipitation to produce the random dispersion, rather than the solution treatment and ageing procedure that was used here. This project was not pursued further because the small precipitation hardening contribution to the yield strength would make unambiguous results difficult to obtain.

4. Scanning electron microscopy of etched fracture surfaces.

The most critical situation is the path of a cleavage crack through the fine carbide dispersions that produce high strength levels. However, this is difficult to investigate experimentally and it is of value to consider first cleavage in the coarser dispersions that result from slow furnace

cooling from the austenitising temperature. Etching in 3% nital permits the scanning electron microscope observation of carbides on fracture surfaces. Figure 2.5 presents some typical results. In figure 2.5a the traces of the two secondary cleavage planes and of the interphase precipitate sheets can be seen for furnace cooled Fe-1V-0.2C fractured at -196°C. The three cleavage planes are orthogonal, and the trace of the precipitate sheets is at 45° to the secondary cleavage planes. This is consistent with fracture on $\{100\}_\alpha$, the expected cleavage plane at this temperature, and precipitate sheets on $\{110\}_\alpha$. Figure 2.5b is for furnace cooled Fe-0.5V-0.1C fractured at -196°C, and this also appears consistent with $\{100\}_\alpha$ cleavage and $\{110\}_\alpha$ precipitate sheets. Figure 2.5c is for furnace cooled Fe-0.5V-0.1C fractured at room temperature. Traces of the precipitate sheets can be seen on the fracture surface, suggesting that the cleavage plane has not changed to $\{110\}_\alpha$. In figure 2.5d the lines of the precipitate sheets are just resolved in Fe-1V-0.2C isothermally transformed at 800°C, and this gives an overlap between this technique and the iron plating technique used in section 7.

5. Fractography of ferrite containing both interphase and Widmanstatten precipitation of vanadium carbide.

Addition of 1% aluminium to the basic Fe-1V-0.2C alloy raises the Ae_3 temperature, and high temperature transformation from austenite to ferrite results in both interphase and Widmanstatten precipitation of vanadium carbide (18). Initial transformation is to ferrite supersaturated with respect to vanadium carbide, which then precipitates to give all three variants of the Baker-Nutting orientation

relationship. These Widmanstatten precipitates are platelets on $\{100\}_\alpha$ and their traces on a section give an indication of the ferrite orientation. Subsequent transformation is by an interphase precipitation mechanism, although the sheets of precipitates often do not lie on $\{110\}_\alpha$ at these high transformation temperatures.

Alloy A2 was isothermally transformed at 900°C and then fractured by impact at room temperature or -196°C. Fracture at -196°C was always consistent with cleavage on $\{100\}_\alpha$, the trace of the fracture being parallel to the traces of one of the precipitate habits (figure 2.6). The path of the cleavage crack was not affected by the presence of the sheets of precipitates. For fracture at room temperature, the normal behaviour was cleavage on $\{100\}_\alpha$, unaffected by the precipitate sheets (figure 2.7a), but there were isolated examples of the trace of the cleavage crack lying parallel to that of the precipitate sheets (figure 2.7b,c).

A further specimen was part broken by impact at room temperature, the impulse being controlled such that the crack stopped two thirds of the way through the specimen. The crack was then filled with Araldite under vacuum and then sectioned to examine the crack path. Figure 2.8 shows the crack tip. The straight portions of the crack are parallel to one of the three Widmanstatten habits that can be seen, and the crack is not parallel to the sheets of interphase precipitation.

6. <u>Orientation of the sheets of vanadium carbide precipitates formed during interphase precipitation in Fe-1V-0.2C.</u>

Alloy A1 was isothermally transformed at 700°C and electron microscope specimens were prepared to determine

the trace of the precipitate sheets. For each area a diffraction pattern and a centred dark field micrograph using a vanadium carbide reflection were taken. In most of the areas examined the precipitates were in straight, parallel sheets and the results of the trace analysis for these areas are shown in figure 2.9, from which it can be seen that the precipitate sheets are probably $\{110\}_\alpha$, as has been found by other workers (3). In some areas the precipitate sheets are not straight, and an example of this is shown in figure 2.10. This deviation from straight precipitate sheets is important because it reduces the probability of cleavage failure occurring by 'unzipping' of the sheets in the way that Edmonds (19) proposed.

7. Transmission electron microscopy of iron plated fracture surfaces of Fe-1V-0.2C.

This technique makes it possible to examine the path of the cleavage crack through the very fine scale microstructures resulting from low isothermal transformation temperatures. It has the disadvantages of difficult specimen preparation and only sampling a very small region of the fracture surface.

Figure 2.11 is a precipitate dark field electron micrograph from a specimen isothermally transformed at 725°C and fractured at -196°C. The sheets of precipitates, which would lie on $\{110\}_\alpha$, are not parallel to the cleavage plane. Figure 2.12 shows a complete analysis of -196°C fracture after isothermal transformation at 800°C. The trace of the precipitate sheets is consistent with their being $\{110\}_\alpha$, and the trace of the cleavage plane is consistent with $\{100\}_\alpha$. In any region of interphase precipitation of

vanadium carbide only one of the three possible variants of the Baker-Nutting orientation relationship will be found. In this particular case it is the variant which lies perpendicular to the cleavage plane. It would appear that, for fracture at -196°C, the interphase precipitate dispersion has no effect on the path of the cleavage crack.

Figure 2.13 shows the fracture at room temperature after isothermal transformation at 790°C. The trace of the cleavage crack is parallel to that of the precipitate sheets, suggestive of fracture on $\{110\}_\alpha$. Figure 2.14 presents the results of a series of trace analyses for room temperature fracture after isothermal transformation at 790°C. The convergence on (001) and $(\bar{1}11)$ is a consequence of the zone axes of the diffraction patterns examined. The traces suggest that fracture is probably on $\{110\}_\alpha$ for these conditions, although the cleavage parallel to the precipitate sheets in figure 2.13 is probably fortuitous.

In figure 2.15 the interaction of the cleavage crack with vanadium carbide fibres can be seen in a specimen isothermally transformed at 790°C and fractured at room temperature. The bright field image shows that the ferrite has been heavily dislocated by the passage of the cleavage crack, and this is typical of fracture at room temperature. Fracture at -196°C results in a lower dislocation density, as shown in figure 2.16. This figure also shows the very fine grain size of the electroplated iron layer, this fine grain size being essential to obtain a ductile deposit which will not break off during foil preparation.

Discussion.

It has been shown that the carbide dispersion in these steels is strongly dependent on the isothermal transformation temperature (4), the intersheet spacing (λ) decreasing as the transformation temperature is reduced. The precipitation hardening contribution to the yield strength (σ_p) is related to the intersheet spacing :

$$\sigma_p = k. \lambda^{-n}$$

where n has values in the range 0.45 to 1.1 (18,20,21). The impact transition temperature is dependent on the yield strength, and it has been shown that where the yield strength is increased by precipitation hardening there is a consequent increase in the impact transition temperature (6). From figures 2.2 and 2.3 it can be seen that this effect is large - 0.54°C/MPa for F1,F2,F3 and 0.64°C/MPa for A1. Gladman et al.(22), working on alloys where the precipitation hardening contribution to the yield stress was much less, obtained a value of 0.26°C/MPa. The precipitate volume fractions in the present work are considerably greater than those examined by Gladman, but the precipitate volume fraction effect is probably small compared with that of the increased yield stress. The change in precipitate volume fraction through the series F1 to F3 is significant, but there is apparently no influence on the impact transition temperature.

The precipitates contributing to the strength of the alloys considered by Gladman et al. would have formed mostly on dislocations after transformation to ferrite, although a small amount of interphase precipitation has

been observed in these alloys(23). In contrast, the precipitates strengthening alloys F1-F3 are formed almost entirely by interphase precipitation, resulting in a non-random carbide distribution. Since the rate of change of impact transition temperature with precipitation hardening is so similar in these situations of random and non-random precipitation it can be inferred that the presence of a non-random dispersion does not adversely affect the impact transition temperature.

This inference is further supported by the results for alloy A1 given in figure 2.3. Batte (8) investigated the effect of prolonged ageing of interphase precipitation dispersions of vanadium carbide. For a dispersion formed at 775°C and then aged at that temperature he showed that after an hour there was no evidence of the original aligned dispersion. The precipitates had a variety of morphologies with apparently no specific preferred growth direction, and a few particles coarsened rapidly at the expense of the rest. Grain boundary precipitates always grew most rapidly. It has since been shown that those precipitates within the grains which are in contact with dislocations grow at the expense of the rest (9). The ageing treatments used for alloy A1 are sufficient to progressively break down the non-random carbide distribution resulting from isothermal transformation by interphase precipitation. The rate of change of impact transition temperature with yield stress is almost identical for the aged (0.66°C/MPa) and non-aged (0.64°C/MPa) dispersions. The shift of approximately 100°C in impact transition temperatures produced by ageing is attributed to the coarse grain boundary carbides that

form during ageing. It is well known that coarse carbides in the grain boundaries can have a marked deleterious effect on the impact transition temperature (24). From this it is concluded that the impact transition temperature in these alloys is determined primarily by the precipitation hardening contribution to the yield stress, that the effect of a non-random as compared with a random carbide dispersion is small, and certainly less than the effect of coarse grain boundary carbides.

The fractographic results must be examined in the light of these conclusions. For the complete range of precipitate dispersions, from very coarse to very fine, no evidence was found that the dispersion modified the path of a cleavage crack during fracture at -196°C. Cleavage was apparently always on $\{100\}_\alpha$, unaffected by the sheets of precipitates on $\{110\}_\alpha$, and there was no preference for fracture on the specific $\{100\}_\alpha$ plane on which the interphase precipitated vanadium carbide platelets lay. For fracture at room temperature in the coarse dispersions there was little effect on the cleavage crack path, only isolated examples of the crack propagating parallel to the precipitate sheets being observed. Fracture in fine dispersions at room temperature was often apparently on $\{110\}_\alpha$, this sometimes giving cleavage parallel to the precipitate sheets. This tendency to change from $\{100\}_\alpha$ cleavage at -196°C to $\{110\}_\alpha$ cleavage at room temperature has been observed by other workers (10,25), but the reasons are not fully understood.

Fractographic analysis suggests that, particularly in

the fine dispersions, there is an influence of the precipitate dispersion on the path of the cleavage crack. However, the influence on the resulting mechanical properties is small and it must be concluded that the mechanical properties of steels strengthened by non-random dispersions of vanadium carbide are substantially the same as those with random dispersions. The increase in impact transition temperature imposes a practical limit on the extent to which precipitation hardening can be used to increase the yield strength in low alloy ferritic steels.

Conclusions.

From a series of tests on Fe-V-C alloys and an Fe-Cu model system it is concluded that :-

1. The rate of change of impact transition temperature with increasing yield stress is comparable for random and non-random ("interphase precipitation") dispersions of vanadium carbide in ferrite.

2. The impact transition temperature is primarily dependent on the yield stress, and not on the precipitate volume fraction.

3. The sheets of vanadium carbide precipitates formed by interphase precipitation lie mostly on $\{110\}_\alpha$.

4. It is, in principle, feasible to compare the properties of random and non-random dispersions by using an Fe-Cu model system.

5. The non-random dispersion of vanadium carbide can influence the path of a cleavage crack during fracture at room temperature, but there is no significant change in the mechanical properties.

6. At $-196^{\circ}C$ the dispersion does not affect the crack path.

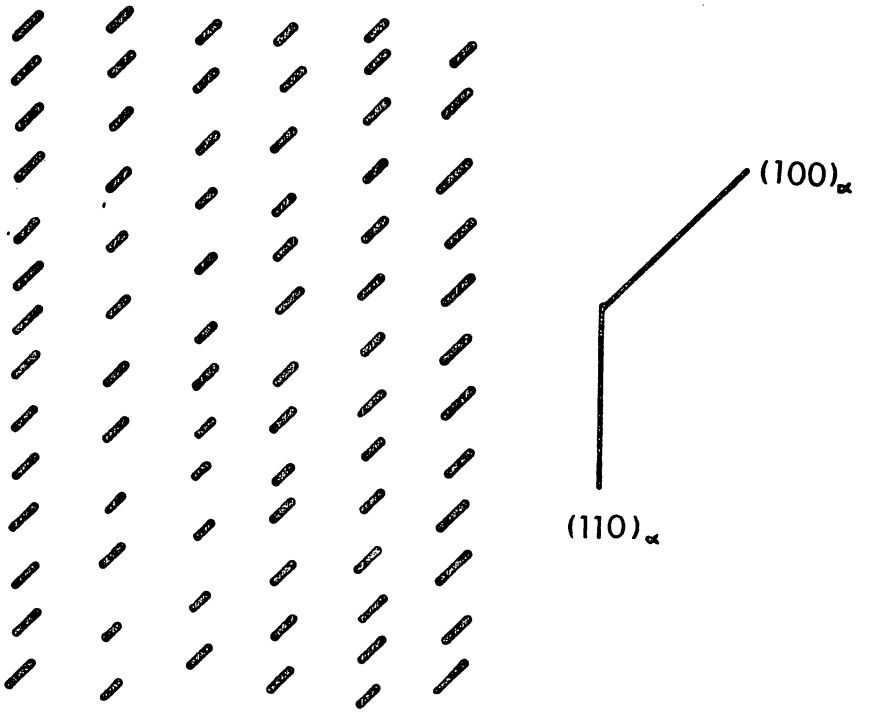

Figure 2.1 Schematic diagram of interphase precipitation.

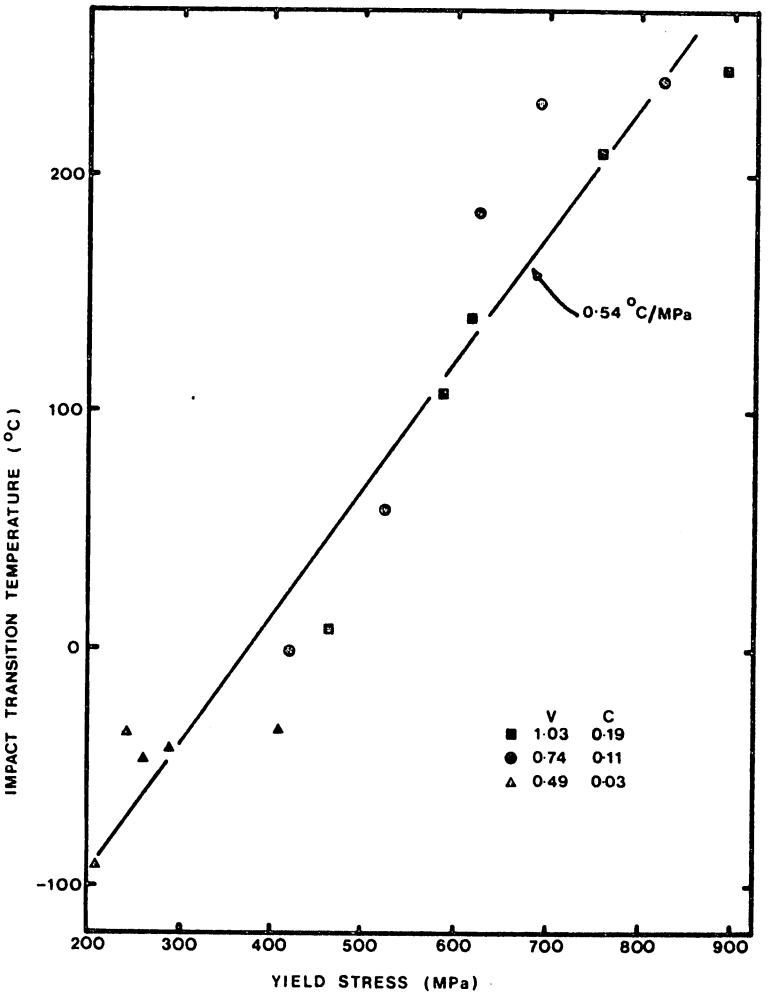

Figure 2.2 The variation of impact transition temperature with yield stress for alloys F1, F2, F3.

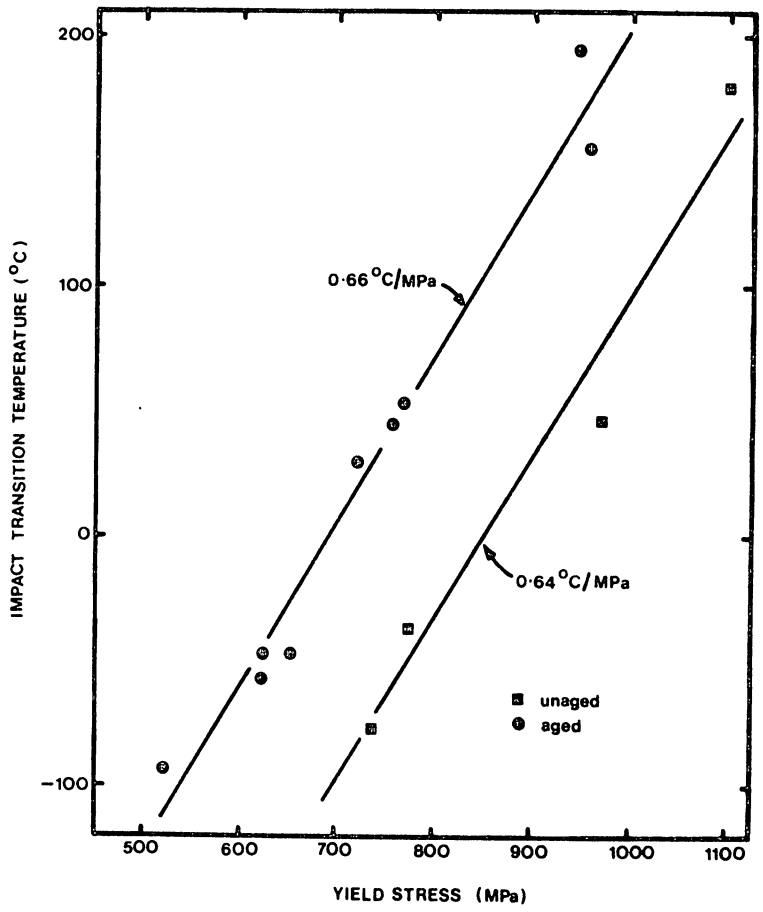

Figure 2.3 The variation of impact transition temperature with yield stress for alloy A1.

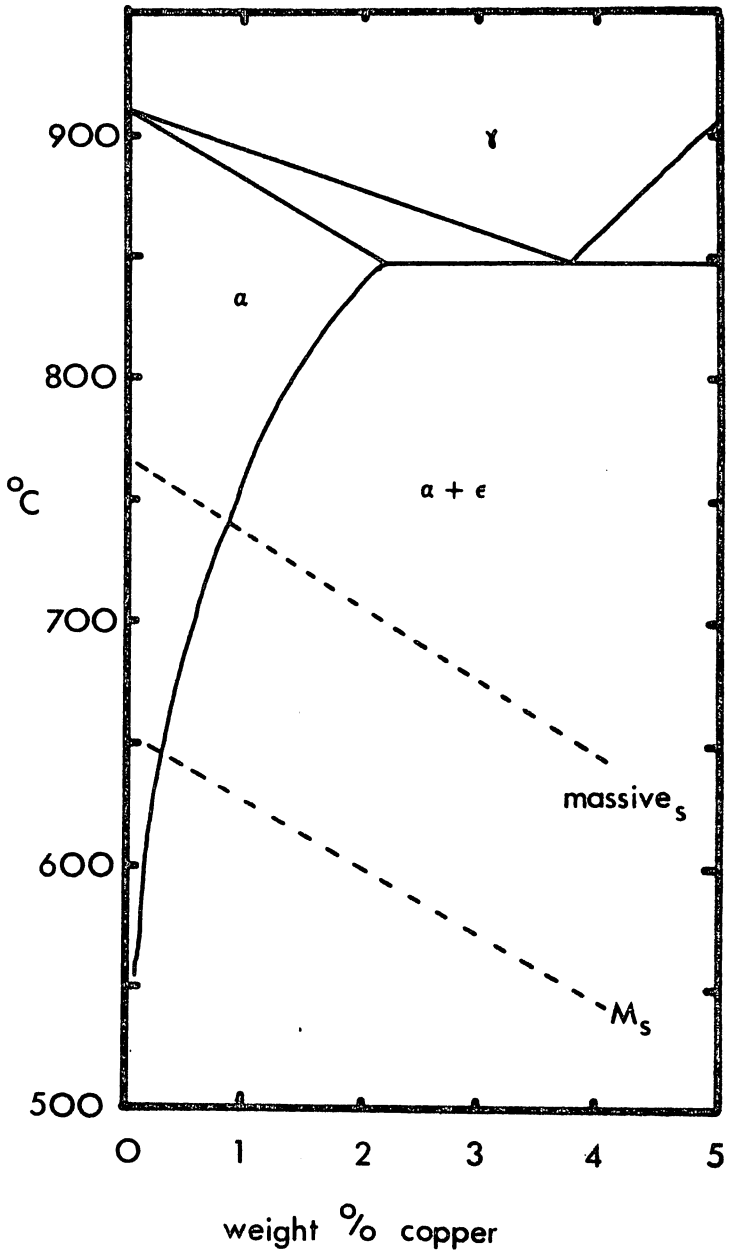

Figure 2.4 The iron-copper phase diagram (after Simensen(13)).

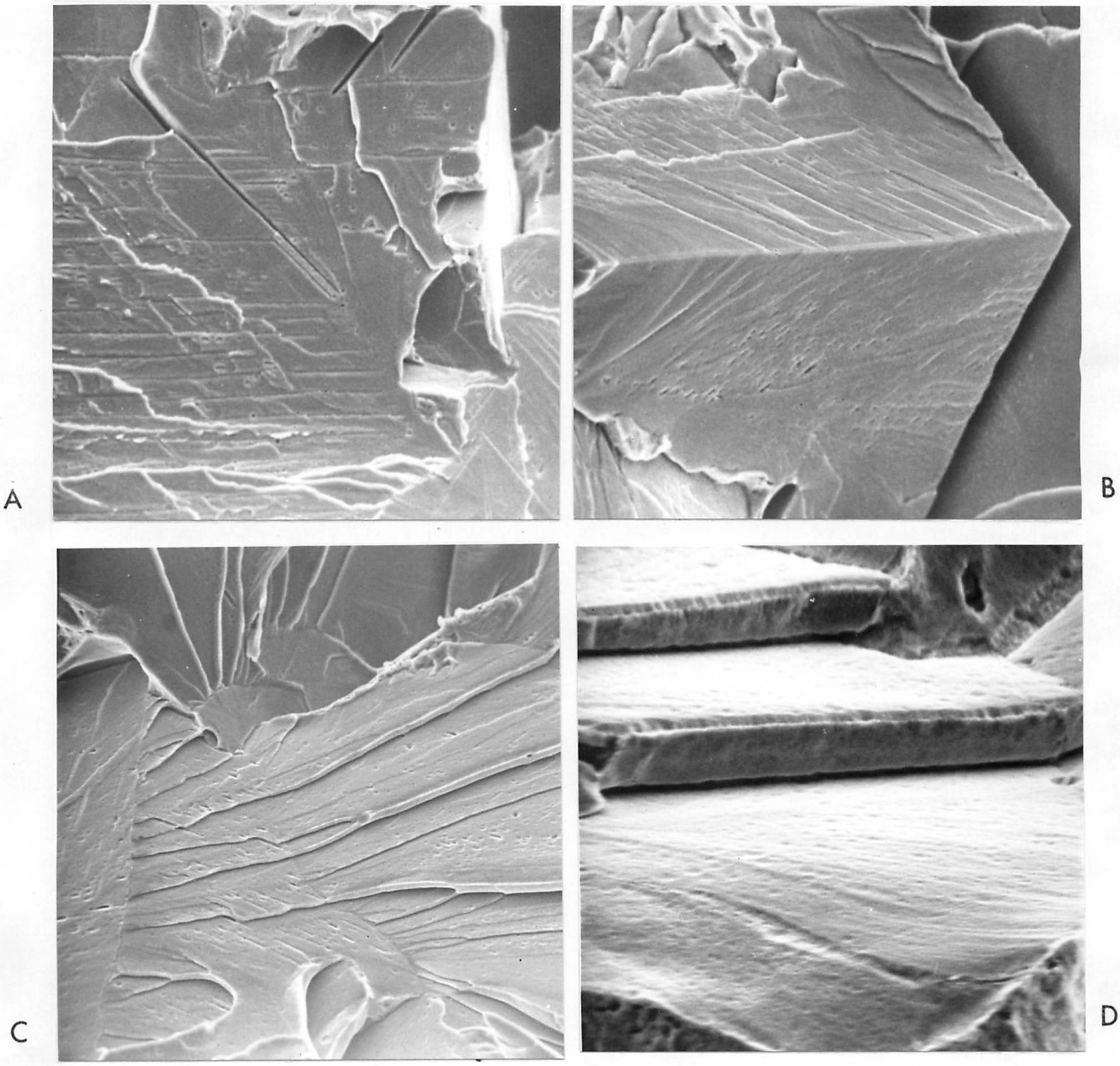

Figure 2.5 Scanning electron micrographs of etched impact fracture surfaces. a) Fe-1V-0.2C, furnace cooled, -196°C fracture (x570), b) Fe-0.5V-0.1C, furnace cooled, -196°C fracture (x1200), c) Fe-0.5V-0.1C, furnace cooled, room temperature fracture (x750), d) Fe-1V-0.2C, transformed at 800°C, room temperature fracture (x4000).

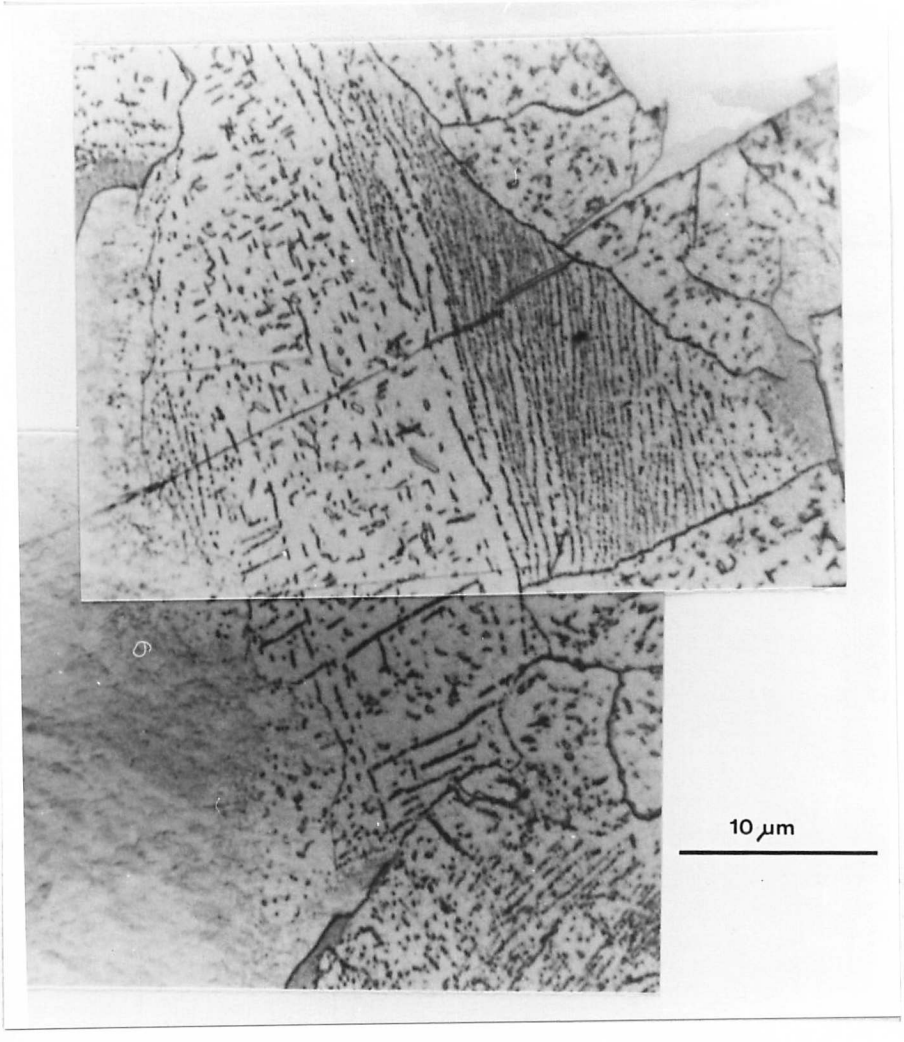

Figure 2.6 Alloy A2 isothermally transformed at 900°C and fractured at -196°C. Nickel plated fracture surface.

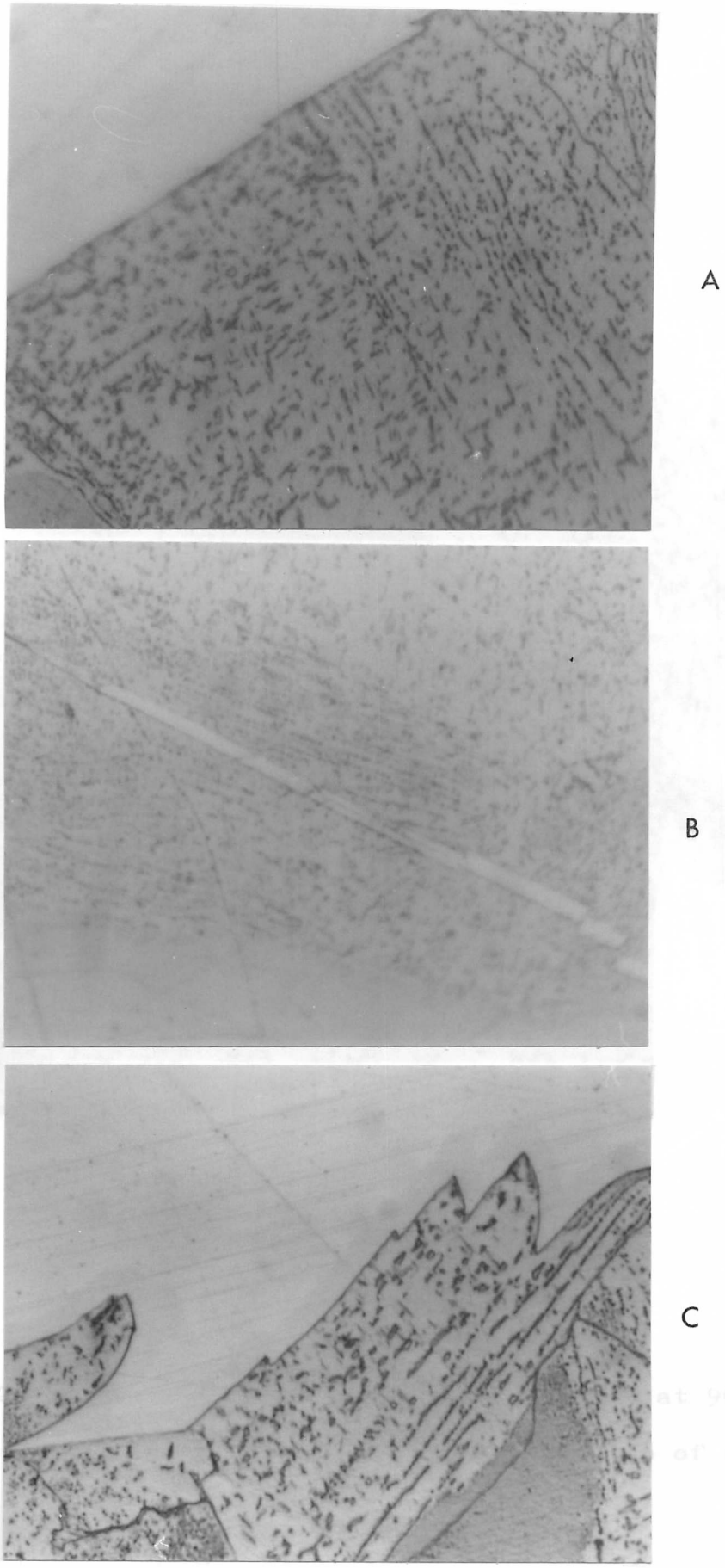

Figure 2.7 Alloy A2 isothermally transformed at 900°C and fractured at room temperature. Nickel plated fracture surfaces (x1800).

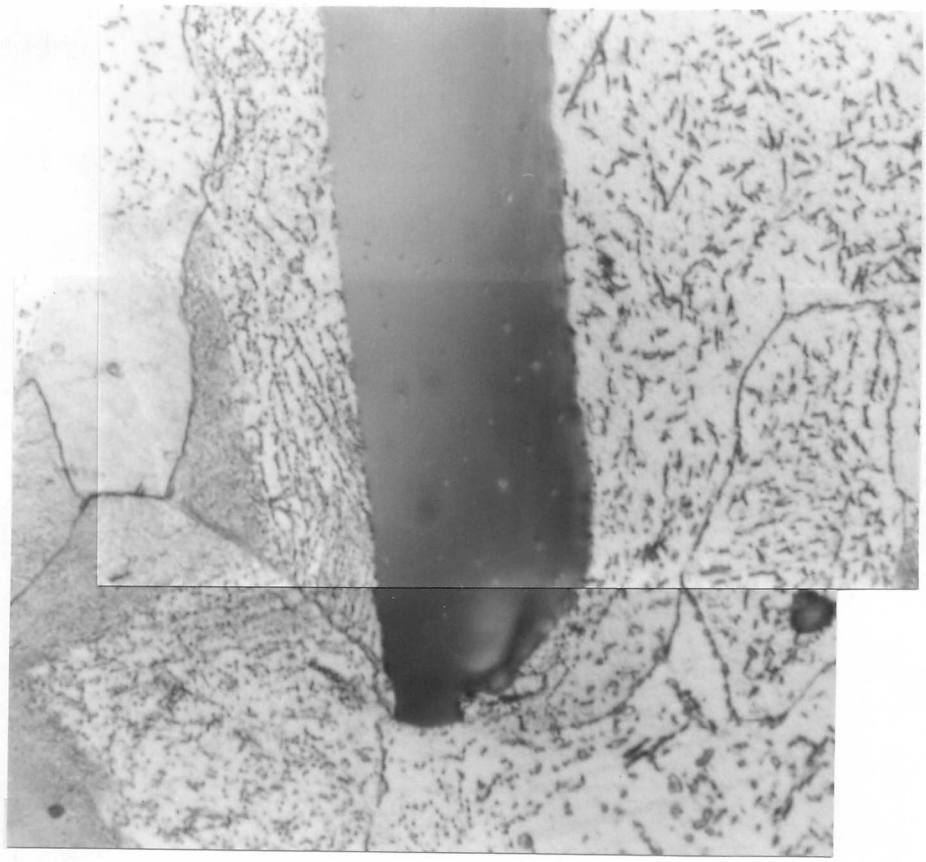

Figure 2.8 Alloy A2 isothermally transformed at 900°C and fractured at room temperature. Tip of arrested crack (x1800).

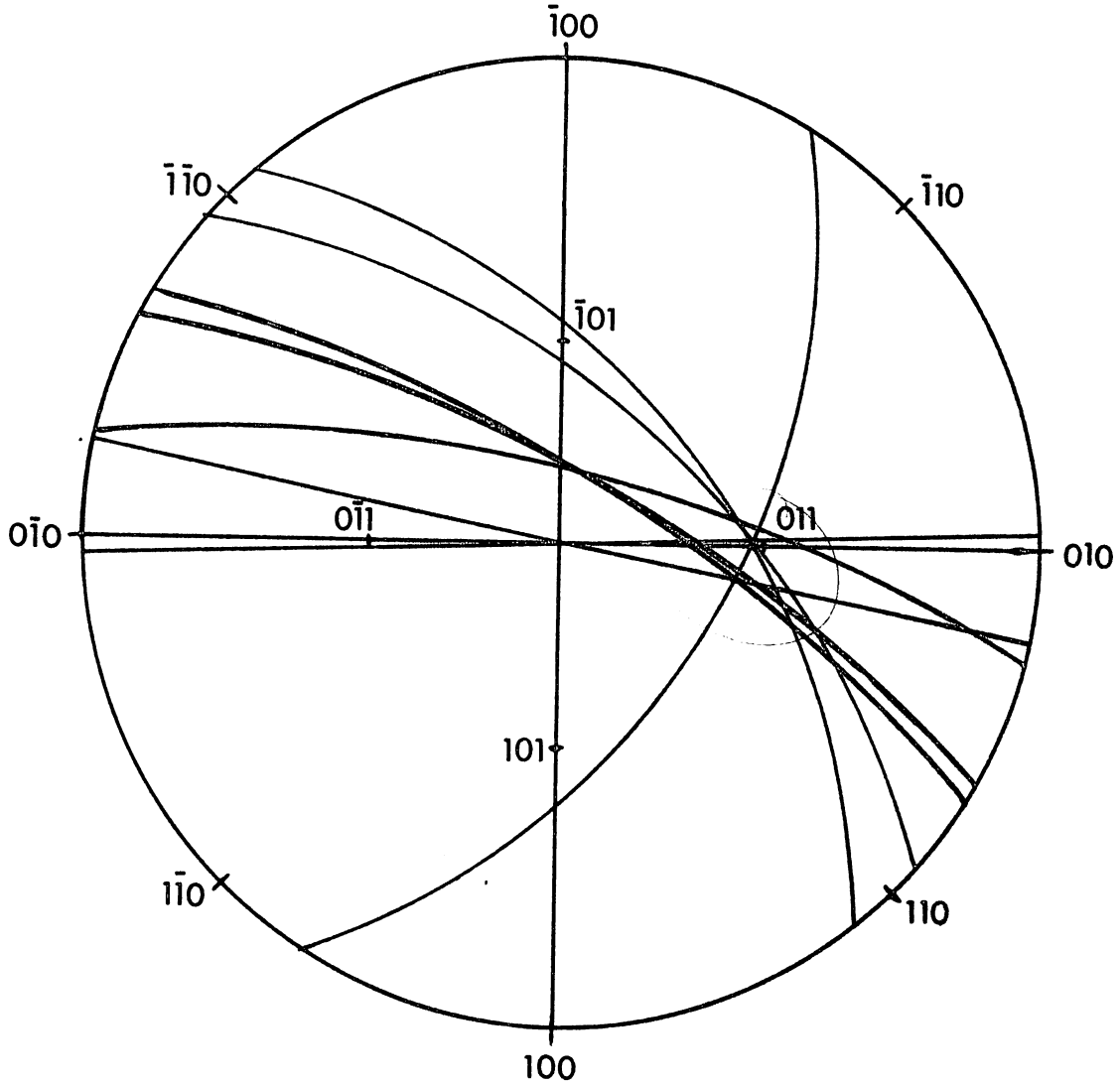

Figure 2.9 Trace analysis of the sheets of vanadium carbide precipitates formed in Fe-1V-0.2C by isothermal transformation at 700°C.

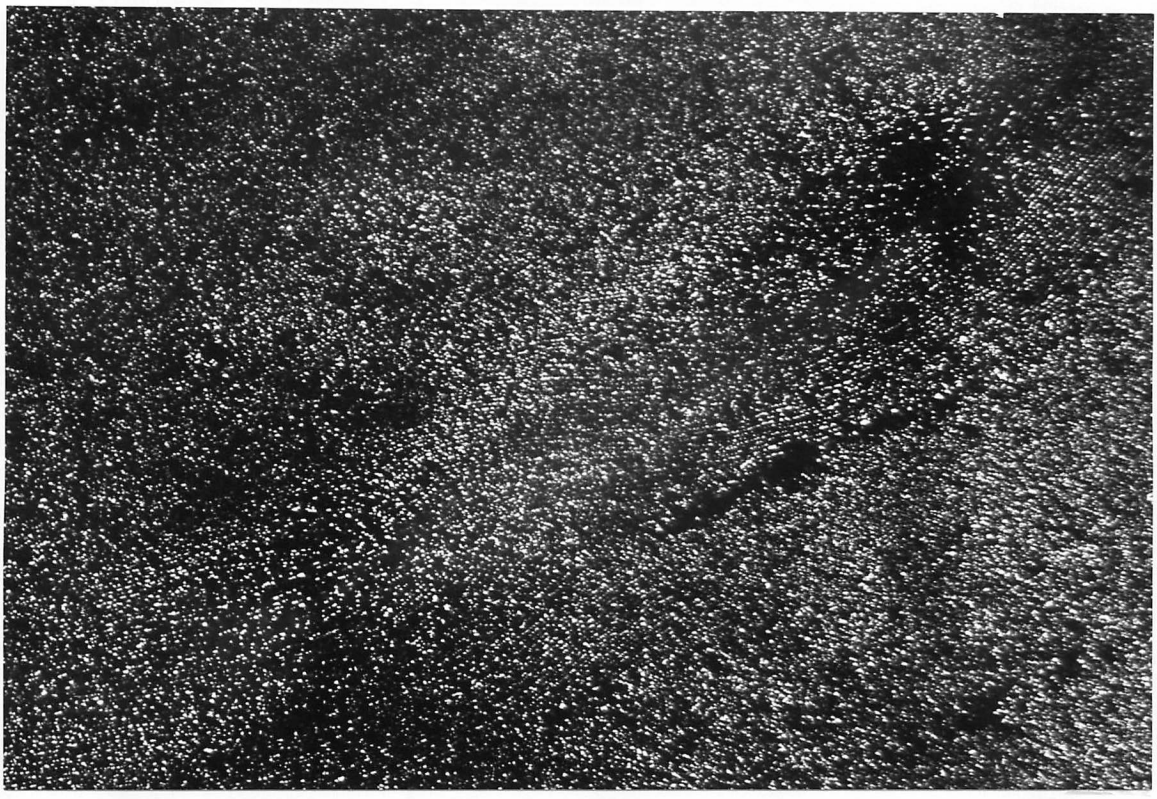

Figure 2.10 Transmission electron micrograph of Fe-1V-0.2C isothermally transformed at 700°C showing the bent precipitate sheets that are found in some regions (x44,000).

Figure 2.11 Transmission electron micrograph of iron plated fracture surface of Fe-1V-0.2C isothermally transformed at 725°C and fractured at -196°C (x30,600).

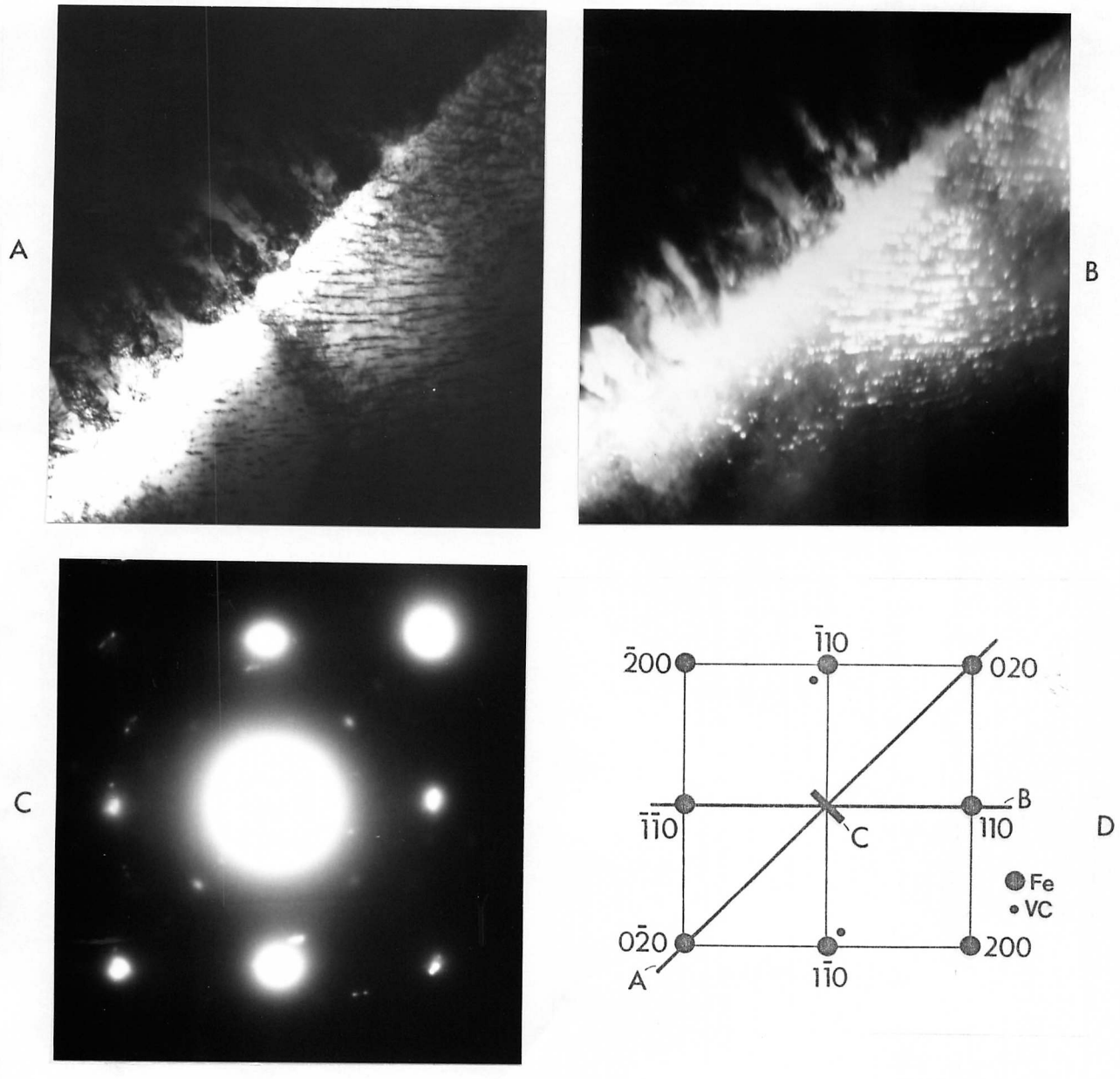

Figure 2.12 Transmission electron micrographs of iron plated fracture surface of Fe-1V-0.2C transformed at 800°C and fractured at -196°C : a) bright field, b) precipitate dark field, c) diffraction pattern and d) schematic diagram of indexed diffraction pattern showing the trace of the cleavage plane (A), the precipitate sheets (B) and the precipitate habit (C) (x21700).

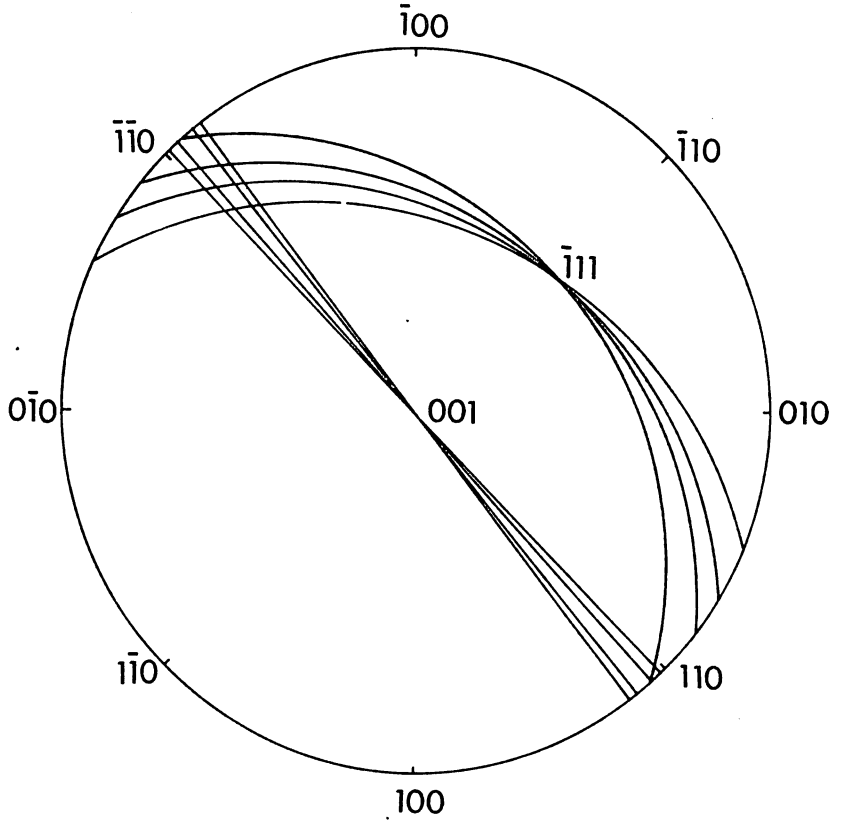

Figure 2.14 Traces of the cleavage planes from transmission electron microscopy of iron plated fracture surfaces of Fe-1V-0.2C isothermally transformed at 790°C, broken by impact at room temperature. N.B. the convergence on (001) and $(\bar{1}11)$ is due to the zone axes of the diffraction patterns examined.

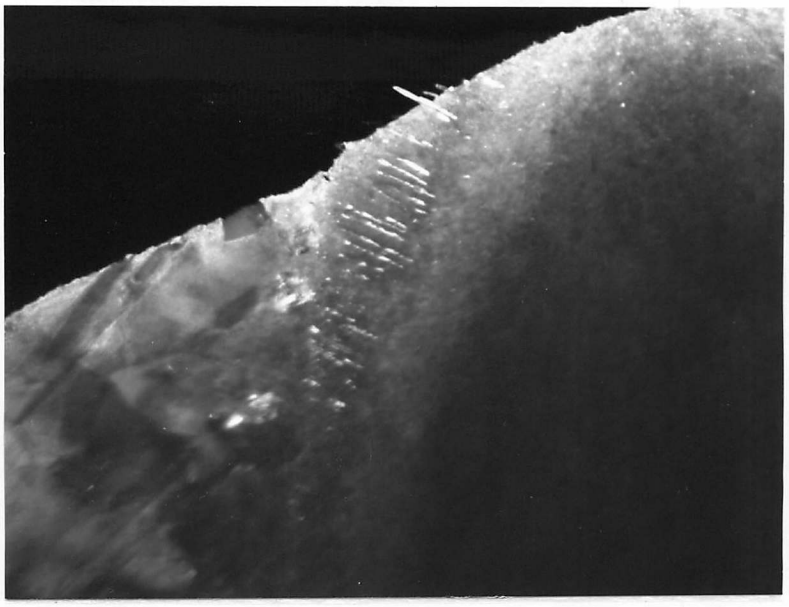

A

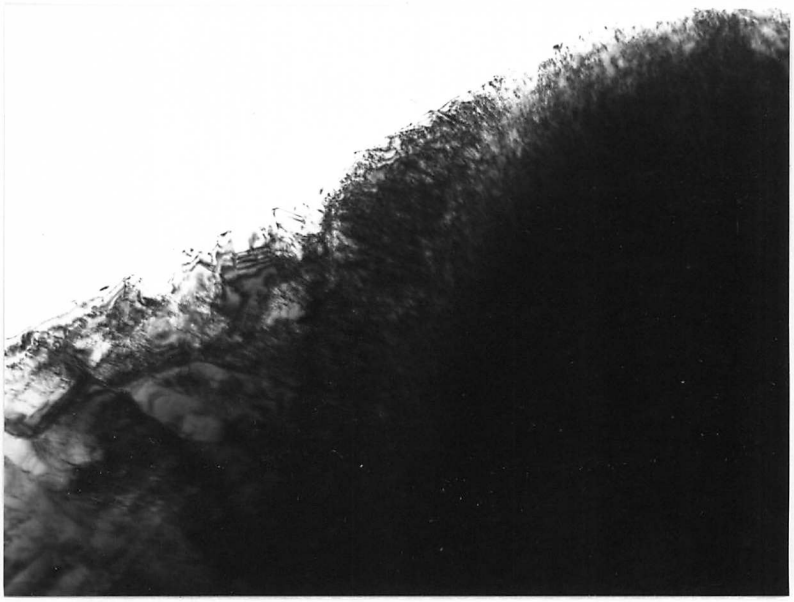

B

Figure 2.15 Transmission electron micrographs of iron plated fracture surface of Fe-1V-0.2C isothermally transformed at 790°C and fractured by impact at room temperature (x23,200).

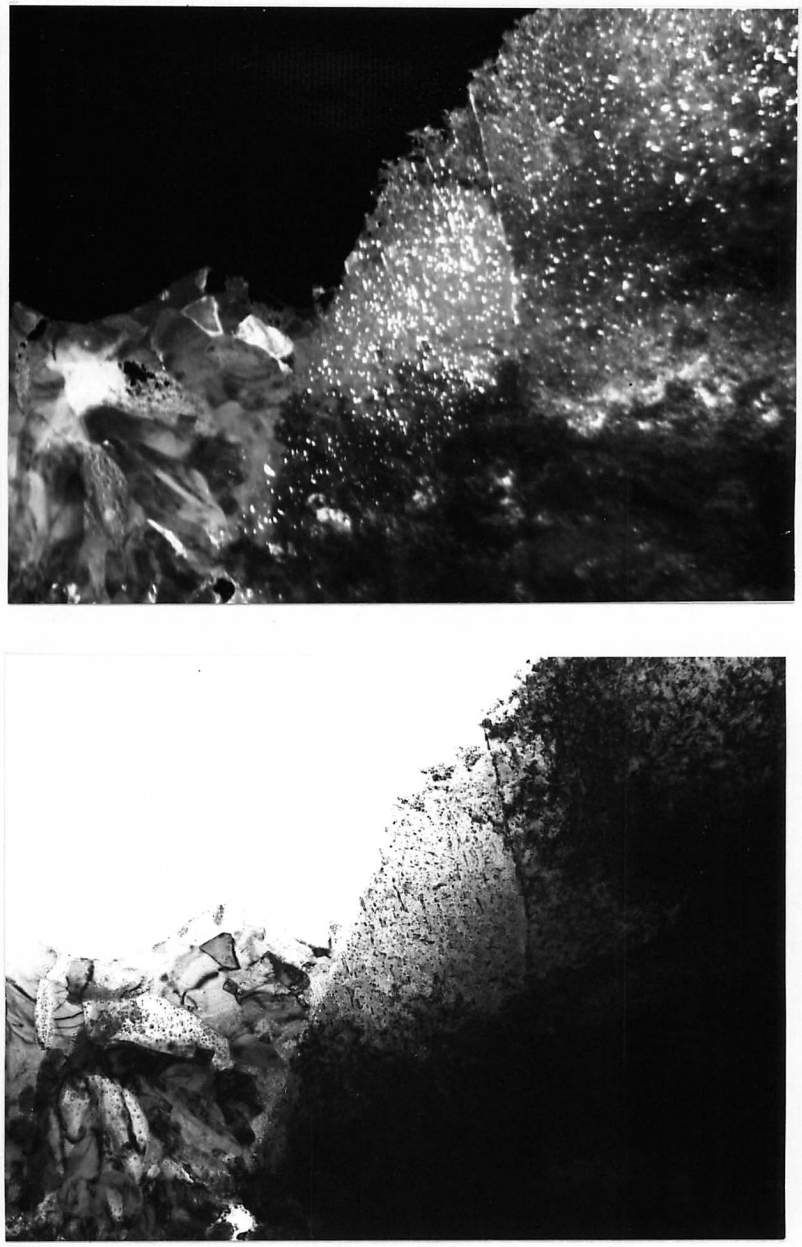

Figure 2.16 Transmission electron micrographs of iron plated fracture surface of Fe-1V-0.2C isothermally transformed at 790°C and fractured at -196°C (x18,400).

CHAPTER THREE.

FATIGUE IN A $\frac{1}{2}$Cr-$\frac{1}{2}$Mo-$\frac{1}{4}$V STEEL.

Introduction.

The work reported here is a development of that described in reference 1 (chapters 3 to 5), where full details of the experimental procedure, the microstructures and the crack growth rate measurements for each microstructural condition are given. This chapter includes further analysis of the earlier results and the results of investigations of the effects of thickness and load ratio on fatigue at intermediate and high crack growth rates in the as received material, and of the effect of microstructure and tensile properties on the fatigue limit. The earlier work showed an unusual load ratio effect, the exponent 'm' in the Paris Law decreasing as the load ratio was increased, and the investigation of the effect of thickness and load ratio was an attempt to understand this. The measurements of fatigue limits were to confirm the apparently conflicting microstructural requirements for good fatigue properties at the threshold ("crack stopping") and at the endurance limit ("crack starting").

Results.

Fatigue crack growth curves for $\Delta K \gtrsim 20 MPa.m^{\frac{1}{2}}$ were determined for the as received material using SEN four point bend specimens with thicknesses of 5, 10 and 20mm. and load ratios of R=0.1, 0.3 and 0.5. The testing frequency was 25Hz.. The fatigue crack was initiated with $\Delta K \sim 25 MPa.m^{\frac{1}{2}}$ and then the loads reduced in stages to a ΔK of typically

$15MPa.m^{\frac{1}{2}}$, sufficient crack growth being allowed at each stage to grow the fatigue crack through the plastic zone associated with the previous load level. The loads were then increased in stages and held constant at a level which was equivalent initially to $\Delta K \simeq 20MPa.m^{\frac{1}{2}}$. The fatigue crack growth curves are presented in figure 3.1, and figure 3.2 shows the results of a regression analysis of the linear region of each curve. There is a tendency for m to decrease with increasing load ratio and with decreasing thickness.

S-N curves were determined for two microstructural conditions, and the results are shown in figure 3.3. The fatigue limit for a quenched and tempered microstructure is higher than that for a ferritic microstructure resulting from isothermal transformation at $750^{o}C$; the ratio of the fatigue limit to the ultimate tensile stress, the fatigue ratio, being 0.50 and 0.40 respectively.

Discussion.

1. The effect of microstructure and tensile properties on fatigue in the intermediate crack growth rate range.

Full details of these tests are given in reference 1 chapter 4, and figure 3.4 summarises the results for the exponent m in the Paris Law as a function of load ratio, yield stress and K_{max} at final instability (an approximate measure of K_{IC}). Figure 3.4 shows that the exponent m in the Paris Law is reduced as yield stress and K_{max} at instability are increased, the change being most marked at R=0.1. Ritchie (26) plotted results from his own and previous work to show that there was a clear correlation between m and

K_{IC}. The trend was for m to decrease as K_{IC} was increased, the increase in m for $K_{IC} < 80 MPa.m^{\frac{1}{2}}$ being particularly marked. This increase in m is attributed to static modes of failure occurring in association with normal striation growth mechanisms (27). In the present work the isolated incidence of a cleavage static mode has been observed in the ferritic microstructures and this may account for some of the change in m.

Figure 3.4a shows that the exponent m is reduced as the yield stress is increased. The various theoretical continuum fatigue crack growth laws (28-32) predict a strong dependence of the fatigue crack growth rate on the material yield stress (σ_y), with the growth rate proportional to σ_y^{-1}, σ_y^{-2} or σ_y^{-4}. It is predicted that the growth rate should be greatly reduced by increasing the material yield stress. Some workers have shown that there is no effect of yield stress on the fatigue crack growth rate (33,34), and others have found that where crack propagation is by a purely striation mechanism then an increase in yield stress results in a small decrease in the crack growth rate (35,36). Lindley et al. (37) found that for various steels in which the yield strength changed by a factor of seven, the change in crack growth rate by the striation mode was only a factor of two. In some cases (38) an increase in yield stress has resulted in an increase in growth rate. It is clear that the observed yield stress effect is always less than that theoretically predicted, and the reasons for this are not understood. Part of this discrepancy is removed by considering the cyclic rather than the monotonic

yield stress. In certain high yield strength materials the effect of the yield stress is offset by the low toughness (32). The results of the present study provide further evidence of a significant reduction in fatigue crack growth rate as the yield stress is increased.

2. <u>The influence of thickness and load ratio on fatigue in the intermediate crack growth rate range</u>.

For the entire range of microstructural conditions, yield stresses and toughnesses it was found that the exponent m for tests at R=0.1 was greater than for tests at R=0.4 (figure 3.4). For the as received material, tested over a range of thicknesses and load ratios, the general trend was also for m to decrease with increasing load ratio (figure 3.2). This reduction in m with increasing load ratio does not agree with much of the published literature. It has been shown that, for fatigue crack growth in the continuum region by a purely striation mechanism, there is generally little effect of load ratio (39). In many cases, however, there is an increase in m with increasing load ratio due to the contribution of static modes of failure to the overall crack growth rate (27,40).

The following paragraphs show that the explanation for the results obtained here can not be found in deviations from ideal plane strain deformation due to crack closure, general yield or increasing plane stress deformation, and it is hoped that further work will provide an explanation for the load ratio effect found in the present study.

When crack closure occurs the effective ΔK at the crack tip is less than that nominally applied and consequently

the fatigue crack growth rate is reduced (41). Crack closure measurements on steel specimens tested in tension have shown that closure at K_{min}, the minimum value of K in the fatigue cycle, is found only in the surface plane stress regions, and not in the interior plane strain regions (42). It was suggested that this accounted for the observed curvature of the crack growth front in fatigue specimens. Irving et al. (43) showed that, for steel specimens, closure in bend specimens was not significant when tested in plane strain in air. For tension specimens they also showed that the extent of closure would be greatly reduced by increasing the applied load ratio or the applied ΔK. For the bend specimens used in the present work it is therefore concluded that closure effects would not be significant.

The effect of general yield of the fatigue specimen is to increase the fatigue crack growth rate (35,44). The general yield stress is greater for thick than for thin specimens, so that thin specimens can show greater fatigue crack growth rates as general yield is approached (44-46). Increasing the load ratio brings the conditions closer to general yield, and so the general yield contribution to the effect of increasing load ratio on m would be to increase m. The opposite effect of load ratio on m has been observed here. Increasing the yield stress of the material will delay the onset of general yield to higher ΔK values, and may then give lower values of m for high strength materials, as shown in figure 3.4a.

It is difficult to isolate the effect on the fatigue crack growth rate of a deviation from ideal plane strain

to plane stress loading. In many specimen designs the effect will be masked by the approach to general yield. Crack closure effects will also become more significant in plane stress loading (42). Some theoretical analyses show that the plane stress crack tip displacement is greater than that for plane strain (47,48) and this should result in faster fatigue crack growth rates in plane stress. However, Griffith and Richards (44) showed that the experimental growth rate was not affected by a change from plane strain to plane stress loading.

3. The relationship between the parameters m and C in the Paris Law.

Recently it has been realised that there is an empirical relationship connecting the parameters C and m (49,50) :

$$m = x \log C + y \qquad 3.1$$

McCartney and Irving (51) have shown, by dimensional arguments, that the linear relationship between m and logC in equation 3.1 is a necessary consequence of the Paris Law. Niccolls (50) analysed data from several sources and showed that for a wide range of steels (yield stress 433-1688 MPa, fracture toughness 27.5-220 $MPa.m^{\frac{1}{2}}$) tested under a variety of conditions the results for m and log C all fitted the same line. An almost parallel line was found for a limited number of aluminium alloys. Bailon et al. (52) tested a series of aluminium alloys and also found a linear correlation between m and log C. They found that the load ratio was the only experimental variable to affect this relationship. Loading cycle, specimen thickness and type, frequency and environment had no effect. Tanaka and Matsuoka

(53) report results for a series of steels tested in zero-to-tension loading and show a linear relationship between m and log C. They attempt to explain this relationship by a crack closure approach, but this must be questioned because Irving et al. (43) have shown that crack closure effects in steels in such conditions are minimal.

Values of m and log C were calculated from the results of all the fatigue tests on the $\frac{1}{2}$Cr-$\frac{1}{2}$Mo-$\frac{1}{4}$V steel so that their relationship could be examined over a range of material variables (microstructure, yield strength and toughness) and of experimental variables (thickness, load ratio and frequency). Figure 3.5 shows the results of a series of tests at constant thickness (B= 10mm.) and frequency (40Hz.) for the complete range of microstructures and yield stresses, at load ratios of 0.1 and 0.4. Regression analysis results in the equations :

R=0.1	$m = -0.644 \log C - 2.729$	3.2
R=0.4	$m = -0.601 \log C - 2.607$	3.3

The lines are almost parallel, but the change in load ratio produces a significant displacement. Analysis for all these results, without considering load ratio, gives :

$$m = -0.724 \log C - 3.458 \qquad 3.4$$

Figure 3.6 presents results for the as received material (yield stress 422 MPa) over a wide range of load ratios (0.1 to 0.5), thicknesses (B= 5 to 20mm.) and frequencies (25, 40Hz.). Regression analysis gives :

R=0.1	$m = -0.611 \log C - 2.388$	3.5
R=0.3,0.4,0.5	$m = -0.663 \log C - 3.020$	3.6
all R	$m = -0.684 \log C - 3.150$	3.7

As in figure 3.5, the line for R=0.1 is slightly displaced from, but almost parallel to, that for the higher load ratios.

These equations should be compared with those for steels derived by other investigators (after standardising to units of mm./cycle and $MPa.m^{\frac{1}{2}}$) :

Niccolls (50) $m = -0.770 \log C - 3.146$ 3.8

Tanaka and Matsuoka (53) $m = -0.643 \log C - 2.661$ 3.9

These results provide further experimental evidence of a linear correlation between m and logC for fatigue crack growth in the intermediate growth rate range. There is also some evidence, figures 3.5 and 3.6, of a slight load ratio effect on the relationship between m and logC in the particular $\frac{1}{2}$Cr-$\frac{1}{2}$Mo-$\frac{1}{4}$V steel tested. Bailon et al. (52) found a pronounced effect in aluminium alloys, but the present results suggest that the effect may be smaller in steels. There is no evidence for yield stress, specimen thickness or frequency affecting the relationship between m and logC. The present results are consistent with those of other studies, although the load ratio effect in steels has not previously been observed.

4. <u>The effect of microstructure and tensile properties on the fatigue limit</u>.

Figure 3.3 shows that the tempered martensite is far more resistant to crack initiation than the isothermally transformed ferrite, whether the comparison is made on an absolute basis (fatigue limit), or a relative basis (fatigue ratio). This is in agreement with the earlier observations (1) of fatigue limits in Fe-1V-0.2C where the tempered martensite

had superior resistance to fatigue crack initiation when compared with isothermally transformed ferrite at the same ultimate tensile stress.

This behaviour should be compared with the effect of microstructure and tensile properties on the threshold (1) where the threshold for the tempered martensite microstructure is less than that for the isothermally transformed ferrite. These different effects on the threshold and the fatigue limit are consistent with those reported in the literature. The fatigue limit is increased by increasing the tensile strength of a material, being typically half the ultimate tensile strength in steels (54), whereas the threshold is reduced by increasing the yield stress (55). For example, typical empirical equations for the dependence of yield stress (σ_y,MPa), fatigue limit (σ_{FL},MPa), and threshold (ΔK_T,MPa.$m^{\frac{1}{2}}$) on grain size (d,m) in mild steel are (56,57) :

$$\sigma_y = 139 + 0.347d^{-\frac{1}{2}} \qquad 3.10$$

$$\sigma_{FL} = 153 + 0.174d^{-\frac{1}{2}} \qquad 3.11$$

$$\Delta K_T = 3.8 + 1.14x10^3 d^{+\frac{1}{2}} \qquad 3.12$$

It is clear that σ_y and σ_{FL} are related to $d^{-\frac{1}{2}}$ and ΔK_T to $d^{+\frac{1}{2}}$, i.e. there is a basic microstructural difference governing the threshold for crack propagation ΔK_T and the threshold for crack initiation σ_{FL}.

The practical implications of these opposing microstructural requirements for good resistance to fatigue crack initiation (high fatigue limit) and good resistance to fatigue crack propagation (high threshold) should be underlined. Materials with high strength and good toughness will generally have a high fatigue limit but a low threshold.

Conclusions.

From various fatigue tests on a $\frac{1}{2}$Cr-$\frac{1}{2}$Mo-$\frac{1}{4}$V steel it is concluded that :

1. The exponent m decreases with increasing yield strength and toughness, the changes being greater at R=0.1 than at R=0.4 (N.B. the microstructure changes from ferrite to bainite to martensite in this sequence).

2. The exponent m in the Paris Law for the continuum region is greater for tests at R=0.1 than for tests at R=0.4 over the whole range of microstructures, yield stresses (285-834MPa) and apparent toughnesses (72-165MPa.$m^{\frac{1}{2}}$).

3. There is a slight decrease in m at each load ratio when the specimen thickness is reduced. This could not be explained by arguments of crack closure, general yield or the onset of plane stress deformation.

4. There is a linear relationship between m and logC for fatigue crack growth in the intermediate growth rate range over a wide range of yield strengths, thicknesses and load ratios. There is a slight load ratio effect on this linear relationship.

5. Tempered martensite gave a low threshold and a high fatigue limit, whereas precipitation-hardened ferrite gave a high threshold and a low fatigue limit. This indicates the conflicting requirements for resistance to fatigue crack initiation and to fatigue crack growth in steels.

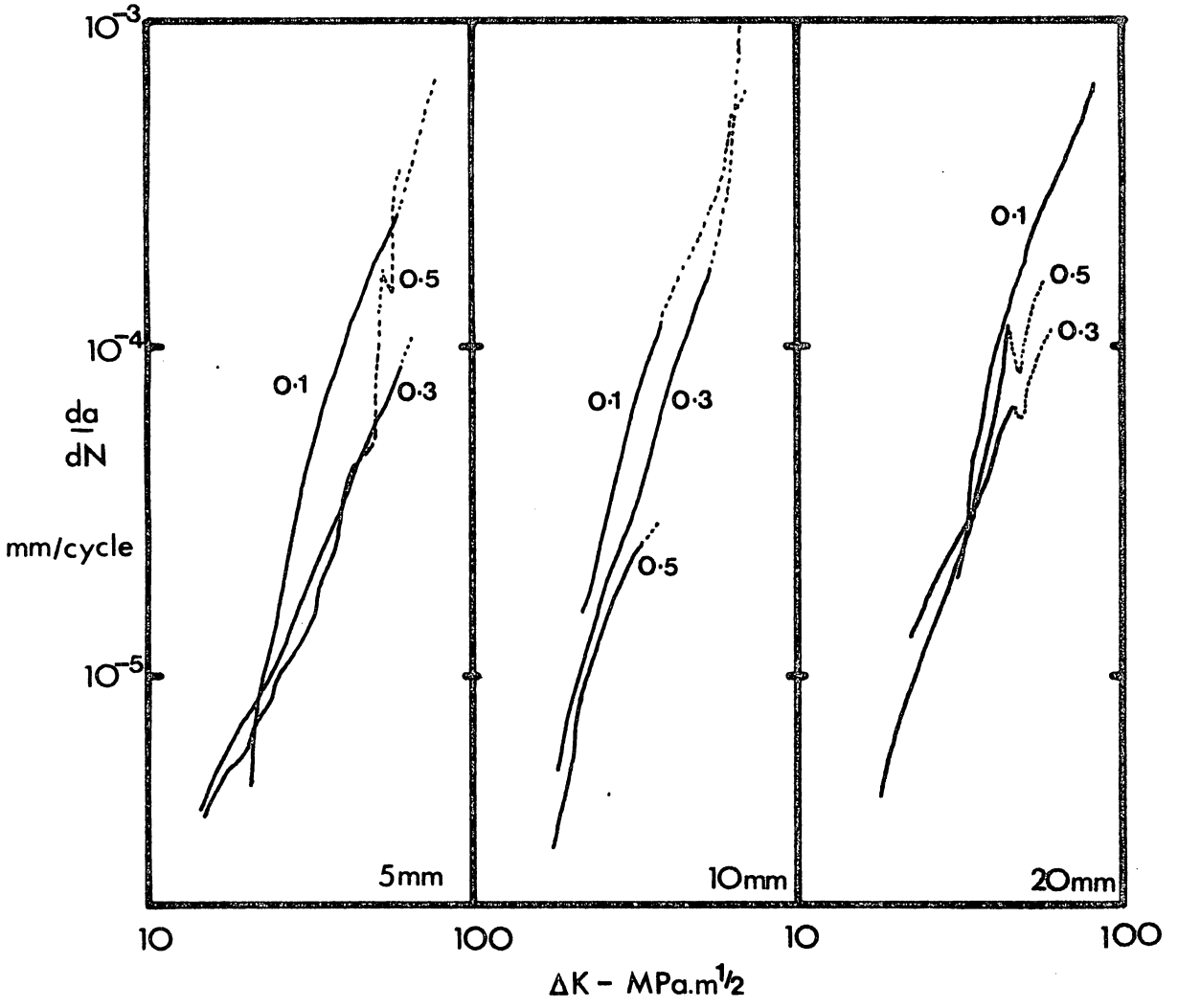

Figure 3.1 Fatigue crack growth curves for the as-received material as a function of thickness and load ratio. The full line is the portion of the curve used in the regression analysis.

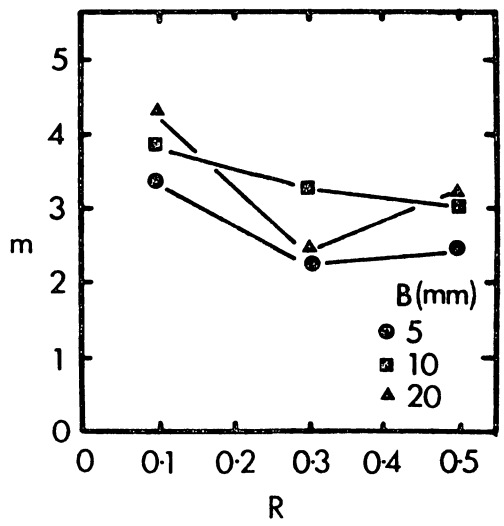

Figure 3.2 The variation of m with thickness and load ratio in the as-received material.

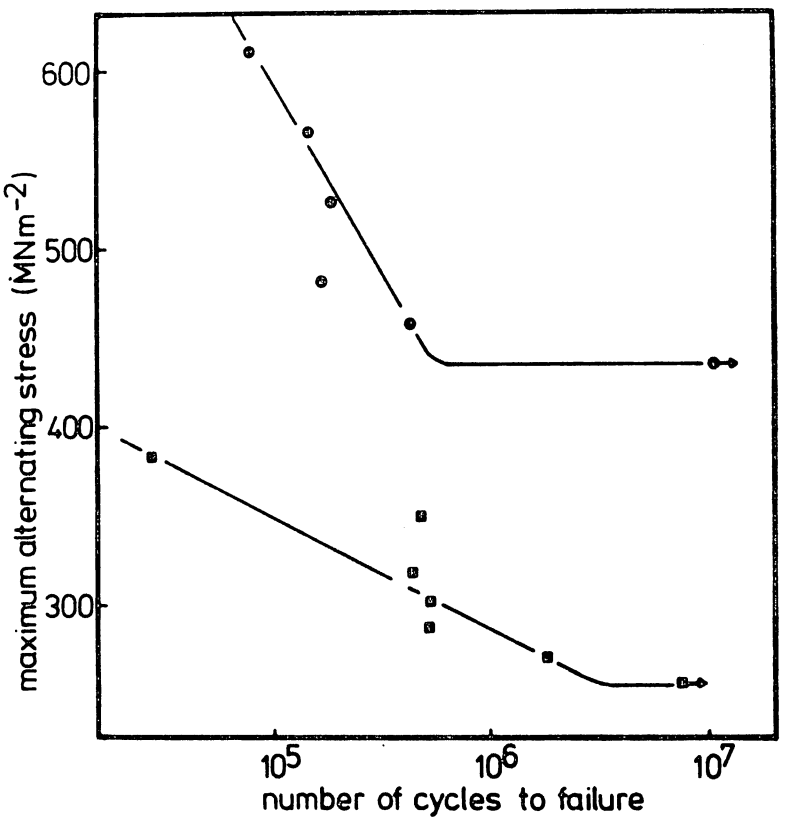

Figure 3.3 S-N curves for fatigue in $\frac{1}{2}$Cr-$\frac{1}{2}$Mo-$\frac{1}{4}$V steel.

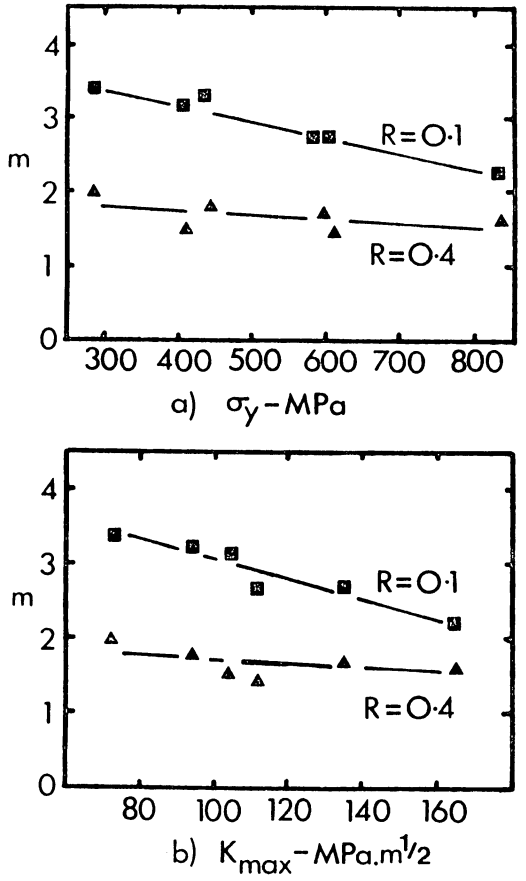

Figure 3.4 The variation of m with yield stress and K_{max} at instability in $\frac{1}{2}$Cr-$\frac{1}{2}$Mo-$\frac{1}{4}$V steel.

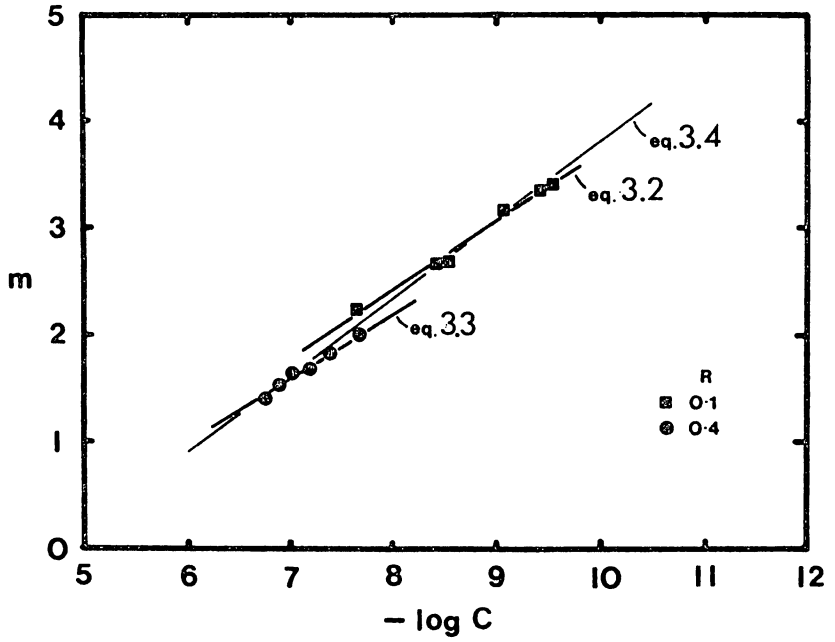

Figure 3.5 The relationship between m and logC for the complete range of microstructures in $\frac{1}{2}$Cr-$\frac{1}{2}$Mo-$\frac{1}{4}$V steel.

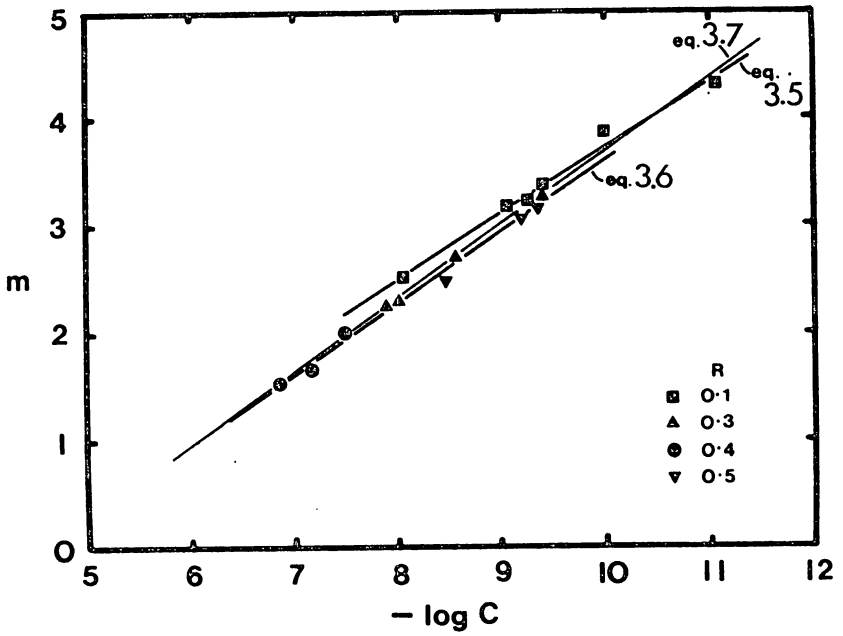

Figure 3.6 The relationship between m and logC for the as-received $\frac{1}{2}$Cr-$\frac{1}{2}$Mo-$\frac{1}{4}$V steel over a range of load ratios and specimen thicknesses.

CHAPTER FOUR.

THE INFLUENCE OF GRAIN SIZE AND YIELD STRENGTH ON THE THRESHOLD FATIGUE BEHAVIOUR OF AN Fe-Ti-C STEEL.

Introduction.

Fatigue crack growth rate measurements are conventionally plotted as a graph of log da/dN versus log ΔK, giving a sigmoidal curve (26) which shows a threshold for fatigue crack growth. The threshold region is of great practical significance since cracked components spend a significant proportion of their fatigue lives in this region. Thresholds have been observed in a wide variety of materials (58), and the threshold is known to be sensitive to microstructure and mechanical properties (56,59,60), load ratio R (56,59-63) and environment (61,64). The threshold is generally reduced as the strength of the material is increased (59). It has been shown (56) that as the grain size of mild steel is increased the threshold is significantly increased. In high strength quenched and tempered steels the prior austenite grain size has an influence on the threshold level (59,65). A steel subject to cyclic softening (59) gave a slight increase in threshold when the prior austenite grain size was increased, whereas in a steel subject to cyclic hardening (65) this gave a slight decrease in threshold. In type 316 stainless steel an increase in grain size resulted in an increase in the threshold (66). The effect of an increase in load ratio is to reduce the threshold (56,59-63). The sensitivity of a material to changes in load ratio can be expressed as γ in (62) :

$$\Delta K_T = \Delta K_O (1 - R)^{\gamma} \qquad 4.1$$

where ΔK_T is the threshold value at load ratio R, and ΔK_0 the threshold value at R=0. Values of γ in the range 0 to 1 have been determined experimentally (67). The environment has a major influence on fatigue in the threshold region (61), and fracture surfaces from steel specimens fatigued in air in this region show evidence of a corrosion product (60,68). Vacuum threshold levels are greater than those in air (61), and it is found that the load ratio has no effect on the threshold value in vacuum, i.e. $\gamma = 0$ (61).

Ritchie (59) has proposed a model based on hydrogen assisted cracking. Hydrogen is produced by reactions at the crack tip involving water vapour from moist air, and then diffuses ahead of the crack tip to give a reduction in the cohesive strength. The assumption is made that the crack growth per cycle is the distance ahead of the crack tip over which the nominal stress exceeds a critical fracture stress (σ_F). Weiss and Lal (58) showed that :

$$\frac{da}{dN} = a. \left(\frac{\Delta\sigma_N}{\sigma_F}\right)^{(n_F + 1)/n_F} . f(a/w) - \frac{\rho_*}{2} \qquad 4.2$$

where $\Delta\sigma_N$ is the applied stress amplitude, f(a/w) a dimensionless correction factor for the specimen width, n_F the cyclic strain hardening exponent and ρ_* the Neuber microsupport constant, which represents the effective radius of the tip of a sharp crack. Near the threshold $n_F \to 1$ and equation 4.2 reduces to :

$$\frac{da}{dN} = \frac{\Delta K^2}{\pi \sigma_F^{\,2}} - \frac{\rho_*}{2} \qquad 4.3$$

where $\Delta K^2 = \pi a. \sigma_N^{\,2}.f(a/w)$.

Weiss and Lal (58) suggest that the threshold occurs when

$da/dN = \rho_*$, i.e.

$$\Delta K_T = \sqrt{\frac{3\pi\rho_*}{2}} \cdot \sigma_F \qquad 4.4$$

Ritchie includes the reduction in cohesive strength ($\Delta\sigma_H$) due to hydrogen to give :

$$\Delta K_T = \sqrt{\frac{3\pi\rho_*}{2}} \cdot (\sigma_F - \Delta\sigma_H) \qquad 4.5$$

Oriani and Josephic (69) assumed that $\Delta\sigma_H$ is proportional to the hydrogen concentration (C_H) at the point of greatest triaxial tension, so that at equilibrium :

$$\Delta\sigma_H = \alpha C_H = \alpha C_0 \cdot \exp(\bar{\sigma}\bar{V}/R_oT) \qquad 4.6$$

where C_0 is the equilibrium hydrogen concentration in the unstressed lattice, α is an unknown constant, $\bar{V}$ the partial molar volume of hydrogen in iron, $\bar{\sigma}$ the hydrostatic tension and R_o the gas constant. From equations 4.5 and 4.6 :

$$\Delta K_T = \sqrt{\frac{3\pi\rho_*}{2}} \cdot \left[\sigma_F - \alpha C_0 \cdot \exp(\bar{\sigma}\bar{V}/R_oT)\right] \qquad 4.7$$

The hydrostatic tension at the crack tip is given approximately by :

$$\bar{\sigma} = \tfrac{1}{3}(\sigma_{xx} + \sigma_{yy} + \sigma_{zz}) = \alpha_1\sigma_y \ln\left[(1 + x/\rho) + \tfrac{1}{2}\right] \qquad 4.8$$

where x is the distance ahead of the crack tip, ρ the crack tip radius and α_1 a constant (>1). Rewriting equation 4.8 in terms of the plastic constraint factor ($\sigma_{yy_{max}}/\sigma_y$) it follows that $\bar{\sigma}$ is given approximately by :

$$\bar{\sigma} = \alpha_1 (\sigma_{yy_{max}}/\sigma_y - \tfrac{1}{2}) \simeq \sigma_y + 2\alpha_2 K \qquad 4.9$$

where $\sigma_{yy_{max}}/\sigma_y \simeq 1 + \alpha_2(K/\sigma_Y)$ (70,71), α_2 is an empirical constant and α_1 is taken to be 2. Combining equations 4.7 and 4.9 gives :

$$\Delta K_T \simeq \sqrt{\frac{3\pi\rho^*}{2}} \left\{ \sigma_F - \alpha C_0 . \exp\left[\frac{\bar{V}}{R_o T} \left(\sigma_y + \frac{2\alpha_2 \Delta K_T}{1-R} \right) \right] \right\} \qquad 4.10$$

If $(\bar{V}\alpha_2\Delta K_T)/(R_o T(1-R))$ is small equation 4.10 becomes :

$$\Delta K_T \simeq \sqrt{\frac{3\pi\rho^*}{2}} \cdot \left[\frac{\sigma_F - \alpha C_0 . \exp(B\sigma_y)}{1 + \frac{\alpha C_0 \rho^{*\frac{1}{2}} . B' . \exp(B\sigma_y)}{1-R}} \right]$$

where $B = \bar{V}/R_o T = 8.10^{-4}$ $(MPa)^{-1}$ at room temperature, and $B' = (3/2\pi)^{\frac{1}{2}} . \bar{V}/R_o T . 2\alpha_2 = 5.10^{-2}$ $(MPa . m^{\frac{1}{2}})^{-1}$.

It is difficult to evaluate all the parameters in these equations, but they do qualitatively explain many observations of threshold fatigue behaviour in steels. From equation 4.7, if $\bar{\sigma}$ is increased then the local hydrogen concentration will increase and the threshold will be reduced. This is accomplished by raising σ_y or R, and it is found experimentally that increasing σ_y or R reduces the threshold. In equation 4.9, the σ_y term in the expression for $\bar{\sigma}$ dominates the K_{max} term at high yield strengths, suggesting a smaller load ratio effect. This has also been found experimentally (59).

Both microstructure and mechanical properties have a strong influence on the threshold in steels and it is difficult to isolate their effects. Masounave and Bailon (56) investigated the change in threshold with grain size in mild steel, but the yield strength is also dependent on the grain size. This ambiguity can be overcome by using a low alloy ferritic steel in which grain size and yield strength can be controlled independently by changing the precipitation hardening contribution to the yield strength.

Freeman (72) investigated Fe-Ti-C steels which had

been controlled rolled, isothermally transformed or continuously cooled. He showed that it was possible to produce a wide range of yield strengths and grain sizes in these steels. In the present work an Fe-Ti-C steel was heat treated to produce a range of yield strengths and ferrite grain sizes, and the threshold was determined for each microstructure as a function of load ratio. It is then possible to examine the effect on the threshold of a precipitation hardened ferritic microstructure of changing the grain size at a constant yield stress, or of changing the yield stress at a constant grain size.

Experimental details.

The material used in these tests was prepared by the British Steel Corporation as 12.5mm. plate of composition (weight %) 0.05C, 0.26Ti, 0.41Mn, 0.02Si, 0.03Al, 0.02S, 0.008P, 12ppm N, 31ppm O. The ingot was soaked for 90 minutes at 1280°C and then rolled from 102mm. to 12.5mm. thickness, finishing rolling at 930°C. The material was then air cooled.

CTS rather than SEN bend specimens were used for the fatigue tests. This has several advantages. Firstly, the testing machine is more stable for low stress intensities and low load ratios when operating in tension rather than compression - it is possible for bend specimens to fall out of the machine when testing near the threshold at R=0.1. Secondly, since the effective specimen width is increased from 20mm. (figure 4.5, reference 1) to 50mm., any crack growth has a smaller effect on ΔK for the CTS specimen. In the threshold region a CTS specimen under constant load

control gives a very close approximation to constant K control, whereas the SEN bend specimen would necessitate the use of the relatively unstable constant K controller to maintain the same K conditions.

Tensile specimen blanks were cut perpendicular to the rolling direction, and CTS blanks were cut such that the crack propagation direction was parallel to the rolling direction. These blanks were heat treated in muffles and salt pots. A pre-treatment of 30 minutes at 1300°C and water quenching was followed by austenitising for 15 minutes at 1250°C and isothermal transformation at 800°C, 725°C or 600°C, and then air cooling. To minimise oxidation and decarburisation, the CTS blanks were welded into mild steel envelopes for the 1300°C pre-treatment and coated with a refractory layer for austenitisation prior to isothermal transformation. The fatigue specimens were machined to the specifications shown in figure 4.1, and the tensile specimen design was Hounsfield no.11.

Tensile tests were carried out on an Instron at a crosshead speed of 0.05 mm./minute. A 60kN Mand servo-hydraulic testing machine was used for fatigue tests in laboratory air at room temperature. The testing frequency was 100 Hz. and the loads were adjusted periodically to maintain constant K conditions. The stress intensity was calculated from (73) :

$$K_I = \frac{P}{Bw^{\frac{1}{2}}} \left\{ 29.6\ (a/w)^{\frac{1}{2}} - 185.5\ (a/w)^{\frac{3}{2}} + 655.7\ (a/w)^{\frac{5}{2}} - 1017\ (a/w)^{\frac{7}{2}} + 638.9\ (a/w)^{\frac{9}{2}} \right\} \qquad 4.12$$

where P is the applied load, B the specimen thickness and w the specimen width. The crack length was monitored by

a potential drop system which measures crack lengths to 0.1 mm. and changes in crack length to 0.01 mm.. This permits measurements of crack growth rates down to 10^{-8} mm./cycle if there is no detectable crack growth in about 10 hours (i.e. overnight). Cracks were initiated with a ΔK of 20-30 $MPa.m^{\frac{1}{2}}$ and then ΔK reduced in stages until the threshold was reached. At each stage the crack was allowed to grow through the plastic zone associated with the previously applied ΔK. Fatigue tests were carried out with load ratios of 0.1, 0.3 and 0.5.

Tables 4.1 to 4.3 show a typical set of calibrations and calculations used in these tests. Table 4.1 is the calibration curve for this specimen design for the potential drop system, here V_o is the output from the potential drop system before crack growth and dV_a is the change in output as the crack grows. Table 4.2 gives values of Y (the function in brackets in equation 4.1) as a function of a/w. The applied loads are calculated, for this machine and specimen design, from :

$$P\ (\%15kN) = \frac{14.908}{Y} \cdot K = x \cdot K \qquad 4.13$$

and the calculations for specimen H11, tested at R=0.3, are given in table 4.3.

Fracture surfaces were examined after nickel plating and sectioning, taking care to note the crack length, and hence ΔK, to which each area corresponded. Transmission electron microscope specimens were prepared by jet polishing 3mm. diameter discs in a solution of 5% perchloric acid in 2-butoxyethanol at 85V and $-20^{o}C$.

Table 4.1 Values of a/w for dV_a in the range 0-149 mV for V_o=300 mV.

	0	1	2	3	4	5	6	7	8	9
0	3543	3574	3604	3635	3665	3695	3725	3756	3786	3815
10	3845	3875	3904	3934	3963	3993	4022	4051	4080	4109
20	4138	4167	4195	4224	4252	4281	4309	4337	4365	4393
30	4421	4449	4477	4504	4532	4559	4586	4614	4641	4668
40	4695	4722	4748	4775	4802	4828	4854	4881	4907	4933
50	4959	4985	5011	5036	5062	5087	5113	5138	5163	5188
60	5214	5238	5263	5288	5313	5337	5362	5386	5410	5435
70	5459	5483	5507	5530	5554	5578	5601	5625	5648	5671
80	5694	5717	5740	5763	5786	5809	5831	5854	5876	5898
90	5921	5943	5965	5987	6008	6030	6052	6073	6095	6116
100	6137	6158	6179	6200	6221	6242	6263	6283	6304	6324
110	6344	6365	6385	6405	6425	6444	6464	6484	6503	6523
120	6542	6561	6580	6599	6618	6637	6656	6675	6693	6712
130	6730	6748	6767	6785	6803	6821	6839	6856	6874	6891
140	6909	6925	6943	6961	6978	6995	7011	7028	7045	7061

Table 4.2 CTS compliance function (Y) as a function of a/w.

a/w	0	1	2	3	4	5	6	7	8	9
0.300	5.85	5.86	5.87	5.88	5.89	5.91	5.92	5.93	5.94	5.95
0.310	5.96	5.98	5.99	6.00	6.01	6.02	6.04	6.05	6.06	6.07
0.320	6.09	6.10	6.11	6.12	6.14	6.15	6.16	6.18	6.19	6.20
0.330	6.22	6.23	6.24	6.26	6.27	6.28	6.30	6.31	6.32	6.34
0.340	6.35	6.37	6.38	6.40	6.41	6.42	6.44	6.45	6.47	6.48
0.350	6.50	6.51	6.53	6.54	6.56	6.57	6.59	6.60	6.62	6.63
0.360	6.65	6.66	6.68	6.70	6.71	6.73	6.74	6.76	6.77	6.79
0.370	6.81	6.82	6.84	6.86	6.87	6.89	6.91	6.92	6.94	6.96
0.380	6.97	6.99	7.01	7.02	7.04	7.06	7.07	7.09	7.11	7.13
0.390	7.14	7.16	7.18	7.20	7.22	7.23	7.25	7.27	7.29	7.31
0.400	7.32	7.34	7.36	7.38	7.40	7.42	7.43	7.45	7.47	7.49
0.410	7.51	7.53	7.55	7.57	7.59	7.61	7.63	7.65	7.67	7.68
0.420	7.70	7.72	7.74	7.76	7.78	7.80	7.83	7.85	7.87	7.89
0.430	7.91	7.93	7.95	7.97	7.99	8.01	8.03	8.05	8.07	8.10
0.440	8.12	8.14	8.16	8.18	8.20	8.23	8.25	8.27	8.29	8.32
0.450	8.34	8.36	8.38	8.41	8.43	8.45	8.47	8.50	8.52	8.54
0.460	8.57	8.59	8.61	8.64	8.66	8.69	8.71	8.73	8.76	8.78
0.470	8.81	8.83	8.86	8.88	8.91	8.93	8.96	8.98	9.01	9.03
0.480	9.06	9.09	9.11	9.14	9.16	9.19	9.22	9.24	9.27	9.30
0.490	9.32	9.35	9.38	9.41	9.43	9.46	9.49	9.52	9.55	9.57
0.500	9.60	9.63	9.66	9.69	9.72	9.75	9.78	9.81	9.84	9.87
0.510	9.90	9.93	9.96	9.99	10.0	10.1	10.1	10.1	10.2	10.2
0.520	10.2	10.2	10.3	10.3	10.3	10.4	10.4	10.4	10.5	10.5
0.530	10.5	10.6	10.6	10.6	10.7	10.7	10.8	10.8	10.8	10.9
0.540	10.9	10.9	11.0	11.0	11.0	11.1	11.1	11.2	11.2	11.2

Table 4.3 Calculation of loads for specimen H11 tested at R=0.3.

dV_a	a/w	Y	x	ΔK	K_{max}	K_{min}	P_{max}	P_{min}
0	3543	6.56	2.273	18.0	25.71	7.71	58.43	17.52
10	3845	7.05	2.115	16.0	22.86	6.86	48.35	14.51
17.5	4065	7.44	2.004	14.0	20.00	6.00	40.08	12.02
22.5	4210	7.72	1.931	12.0	17.14	5.14	33.10	9.93
27.5	4351	8.01	1.861	11.0	15.71	4.71	29.24	8.77
30.0	4421	8.16	1.827	10.0	14.29	4.29	26.11	7.84
31.5	4463	8.26	1.805	9.5	13.57	4.07	24.49	7.35
34.0	4532	8.41	1.773	9.0	12.86	3.86	22.80	6.84
34.5	4545	8.44	1.766	8.5	12.14	3.64	21.44	6.43
34.5	4545	8.44	1.766	9.0	12.86	3.86	22.71	6.82
35.0	4559	8.47	1.760	9.5	13.57	4.07	23.88	7.16
35.5	4573	8.51	1.752	10.0	14.29	4.29	25.03	7.52
35.5	4573	8.51	1.752	11.0	15.71	4.71	27.52	8.25
36.0	4586	8.53	1.748	12.0	17.14	5.14	29.96	8.98
36.5	4600	8.57	1.740	13.0	18.57	5.57	32.30	9.69
38.0	4641	8.66	1.721	14.0	20.00	6.00	34.43	10.33
40.0	4695	8.80	1.694	16.0	22.86	6.86	38.73	11.62
42.5	4762	8.96	1.664	18.0	25.71	7.71	42.78	12.83
45.0	4828	9.13	1.633	20.0	28.57	8.57	46.65	13.99

Experimental results.

Microstructure and tensile properties.

The material was received in the controlled rolled condition with a 24 μm. ferrite grain size. Isothermal transformation after high temperature austenitisation resulted in precipitation hardened ferrite with a grain size of about 70 μm., figure 4.2 a-d. Interphase precipitation of titanium carbide occurs during the transformation from austenite to ferrite in this material, and figure 4.3 shows a centred dark field electron micrograph of the precipitate dispersion after isothermal transformation at 800°C. Air cooling from 930°C gives a coarser dispersion than this, and isothermal transformation at 725°C and 600°C much finer dispersions. This is reflected in the tensile properties shown in Table 4.4, where the low isothermal transformation temperatures result in higher yield strengths. For the as received material the variation in properties across the plate width was also examined, and the results are presented in figure 4.4. At the edges of the plate the higher cooling rate during air cooling results in higher strength. The value for the yield stress given in Table 4.4 is for the region of the plate where fatigue crack growth occurs in the finished specimens.

Fatigue properties.

The fatigue results are presented as plots of log da/dN versus log ΔK in figures 4.5 and 4.6. Figure 4.5 shows the behaviour of each microstructure in the threshold region as a function of load ratio. Figure 4.6 shows the effect of microstructure on the properties at each load

Table 4.4 Tensile properties.

	YS (MPa)	UTS (MPa)	ϵ_f (%)	RA (%)
as received	411	490	30	83
transformed at 800°C	368	505	30	84
transformed at 725°C	581	708	24	66
transformed at 600°C	681	792	22	52

Table 4.5 Plastic zone sizes at the threshold.

w_{rev} (μm.)	R=0	0.1	0.3	0.5
as received	14.2	12.7	10.1	7.7
transformed at 800°C	33.1	28.2	17.7	11.0
transformed at 725°C	9.2	8.7	7.1	6.4
transformed at 600°C	4.8	-	4.1	3.7
w_{max} (μm.)				
as received	14.2	15.6	20.6	30.8
transformed at 800°C	33.1	34.7	36.1	44.0
transformed at 725°C	9.2	10.7	14.5	25.6
transformed at 600°C	4.8	-	8.4	14.8

ratio. Figure 4.7 shows the dependence of the threshold value on load ratio for each microstructure. The threshold value for each microstructure is reduced as the load ratio is increased. Figure 4.8 presents threshold vaues at R=0, obtained by extrapolation from figure 4.7, as a function of yield stress. At a constant grain size (70μm.) the threshold value is reduced as the yield strength is increased. Reducing the grain size to 24μm. lowers the threshold value at R=0 by 3MPa.$m^{\frac{1}{2}}$. The results of Masounave and Bailon (56) are also plotted on figure 4.8, and they suggest a similar lowering of the threshold value for this grain size reduction. Values of γ are included in figure 4.7, and it can be seen that γ is reduced as the yield strength is increased. For each microstructure and load ratio the plastic zone sizes at the threshold were calculated using (74,75) :

$$w_{rev} = (1/3\pi).(\Delta K/2\sigma_y)^2 \qquad 4.14$$

$$w_{max} = (1/3\pi).(K_{max}/\sigma_y)^2 \qquad 4.15$$

The plastic zone sizes are given in Table 4.5, and it can be seen that there is no correlation between the plastic zone size at the threshold and the ferrite grain size.

Fractography of fatigue crack propagation.

Each fracture surface showed evidence of a corrosion product after fatigue in the threshold region. Above the threshold the coarse grain size isothermally transformed specimens exhibited facets which sectioning proves to be transgranular cleavage facets (figure 4.9a), the cleavage continuing several grain diameters under the fracture

surface. The fine grain size as received microstructure did not produce these cleavage facets. At the threshold (figure 4.9b,c) fracture was transgranular, with some evidence of crack branching.

Discussion.

The results show that, in this titanium steel, the threshold is reduced by increasing the load ratio, and that the threshold at R=0 (ΔK_θ) is reduced by increasing the yield stress or decreasing the ferrite grain size. The load ratio sensitivity (γ) is reduced as the yield stress is increased. Fracture surfaces from coarse grain size ferrite are rougher than those resulting from fine grain sizes, and all fracture surfaces show evidence of environmental interaction in the threshold region.

Ritchie's model for the threshold (59) predicts that the threshold will be reduced by increasing the yield stress or the load ratio, since these increase the hydrostatic tension at the crack tip and so the local concentration of hydrogen, resulting in a lower threshold. The present results give further experimental evidence to support this analysis. Ritchie's model also suggests that load ratio will have a smaller influence on the threshold value as the yield strength is increased, and this effect can be seen in figure 4.7. As the yield strength is increased from 368 to 681 MPa, γ is reduced from 0.8 to 0.2. The model does accurately predict the effects of yield stress and load ratio on the threshold, and the effect of yield stress on γ, for the titanium steel investigated in this

work.

The model does not account for grain size effects on the threshold. Figure 4.8 shows that these effects are very significant. In the titanium steel reducing the grain size from 70μm. to 24μm. reduces the threshold by 3MPa.$m^{\frac{1}{2}}$. In the mild steel investigated by Masounave and Bailon (56) reducing the grain size from 153 to 19μm. reduced the threshold by 9.5MPa.$m^{\frac{1}{2}}$. If the yield stress influence on the threshold in mild steel is comparable to that measured in the titanium steel, then the threshold reduction of 9.5MPa.$m^{\frac{1}{2}}$ is due almost entirely to the change in grain size rather than the consequent change in yield strength.

Various mechanisms have been proposed for the effect of grain size on the threshold value ΔK_0. Masounave and Bailon (56) considered that deviation of the crack in coarse grained ferrite resulted in an effective reduction in the macroscopic fatigue crack growth rate (da/dN). This is reasonable for explaining changes in da/dN above ΔK_0, but it does not account for a threshold change of 9.5MPa.$m^{\frac{1}{2}}$ on changing grain size from 153 to 19μm.. It has been shown (76) that for a crack with a bent tip the true K_I value is less than that for a straight crack. Priddle (66) considered that increasing the grain size from 50 to 330μm. would lower the true K value at the crack tip by a factor of 0.9 because of the crack tip deviation. He also showed (66) that the increase in real crack surface area over that suggested from macroscopic crack length and thickness measurements could account for a further reduction in the true K value at the crack

tip by a factor of 0.8 On increasing the grain size from 50 to 330μm.. His results showed a reduction in the threshold on reducing the grain size of stainless steel which was consistent with these factors. These two effects are not sufficient to explain the change in threshold with grain size in the present work and that of Masounave and Bailon (56), although they undoubtedly contribute to the observed changes. It should be noted that these effects will also influence vacuum threshold measurements, so that measurements of thresholds in both air and vacuum may permit the isolation of environment-grain size interactions from modifications to the true K_I value resulting from crack deviations in coarse grain size materials. It is clear that any realistic model for the threshold in steels must include an environmental effect since there is strong evidence that the threshold is changed by testing in vacuum (61), that fracture surfaces from the threshold region show a corrosion product which is not found away from the threshold region, and also the hydrogen embrittlement model does describe many of the salient points of threshold behaviour, with the exception of grain size effects.

Further work involving threshold determinations in both air and vacuum is needed to elucidate the means whereby material grain size affects the threshold value in steels.

Conclusions.

Fatigue crack growth rates in air in the threshold region have been measured in an Fe-Ti-C steel heat treated to produce a range of ferrite grain sizes and yield strengths.

The following conclusions can be made :

1. For each microstructure the threshold value is reduced by increasing the load ratio.

2. At a constant ferrite grain size the threshold value at R=0 is reduced by increasing the yield strength by precipitation hardening.

3. Reducing the ferrite grain size reduces the threshold value at R=0.

4. The sensitivity of the threshold value to load ratio is reduced as the yield strength is increased.

5. The effects of yield stress and load ratio are consistent with a model based on hydrogen embrittlement from environmental interactions.

6. The effect of ferrite grain size cannot be fully accounted for using models based on crack deviations in coarse grain size materials.

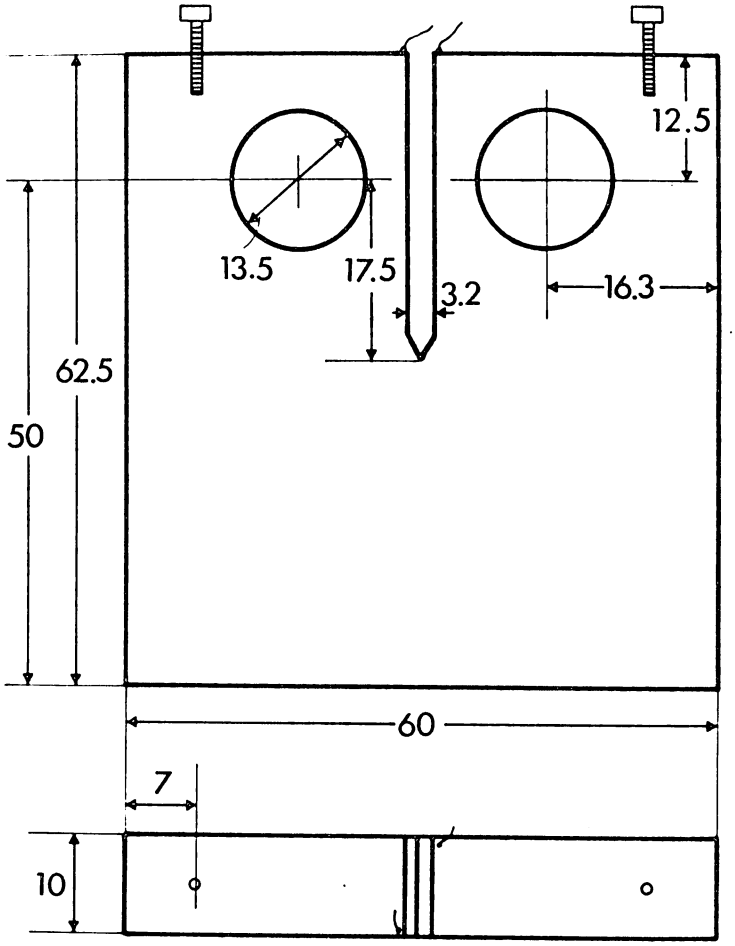

Figure 4.1 Dimensions (mm.) of the CTS fatigue specimens.

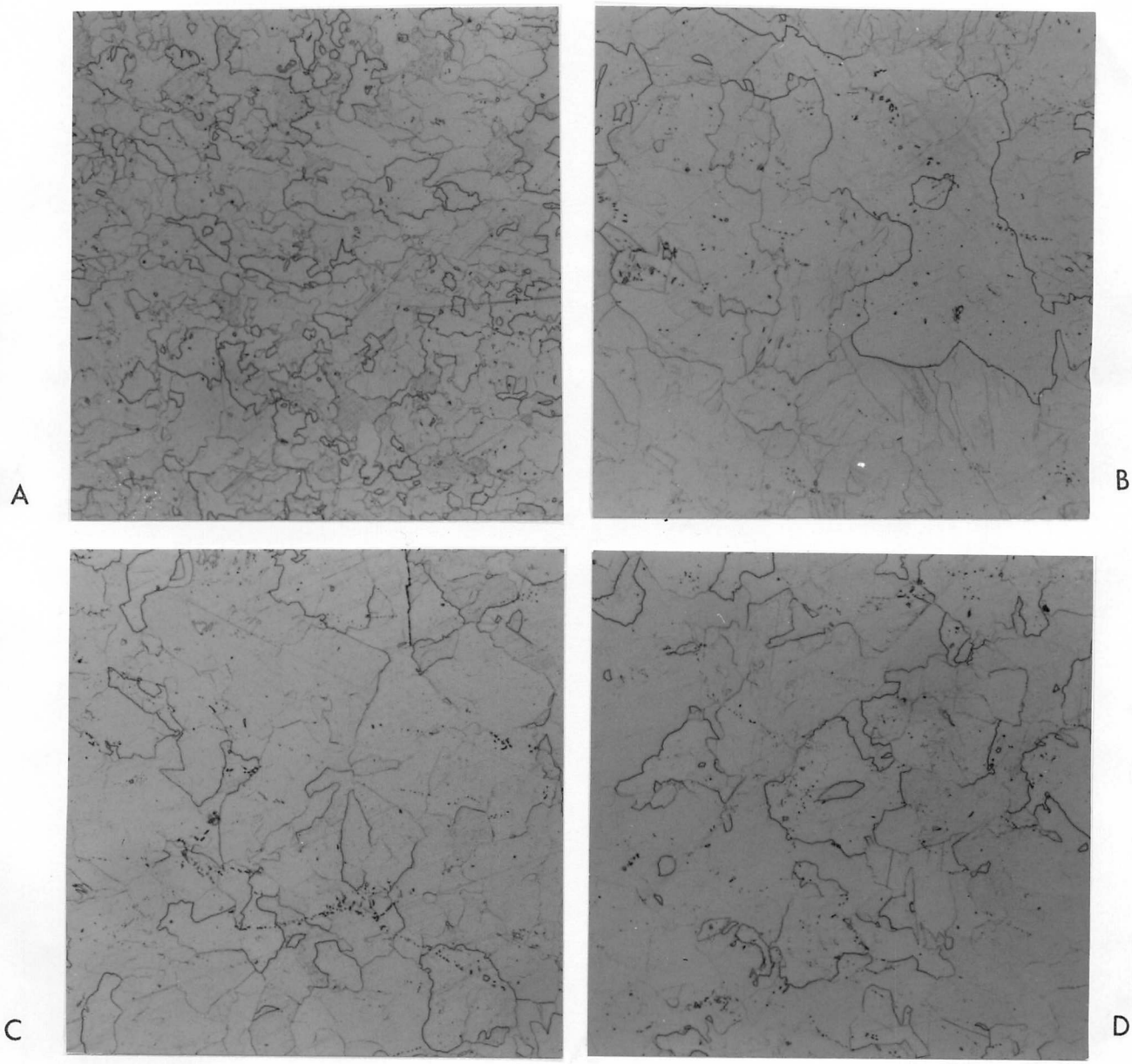

Figure 4.2 Optical micrographs of Fe-Ti-C : a) as received, b) transformed at 800°C, c) transformed at 725°C, d) transformed at 600°C (x230).

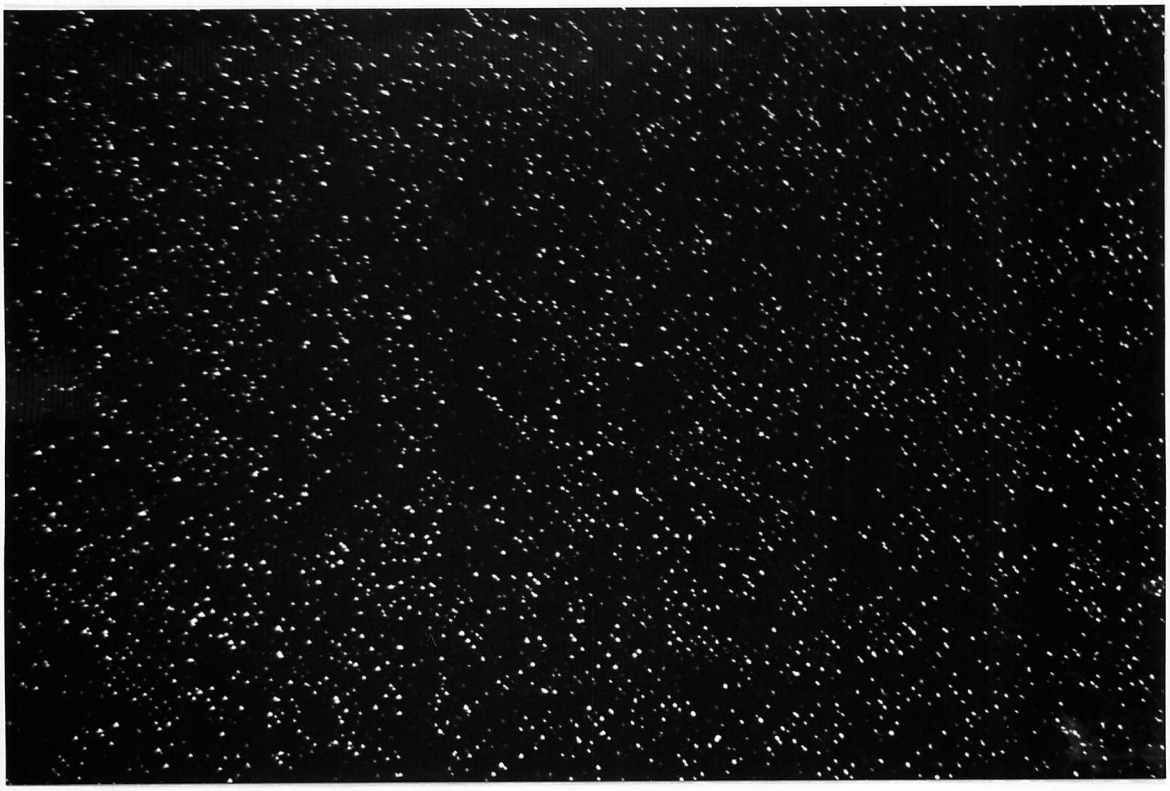

Figure 4.3 Centred dark field electron micrograph, using a titanium carbide reflection, of material isothermally transformed at 800°C (x30,000).

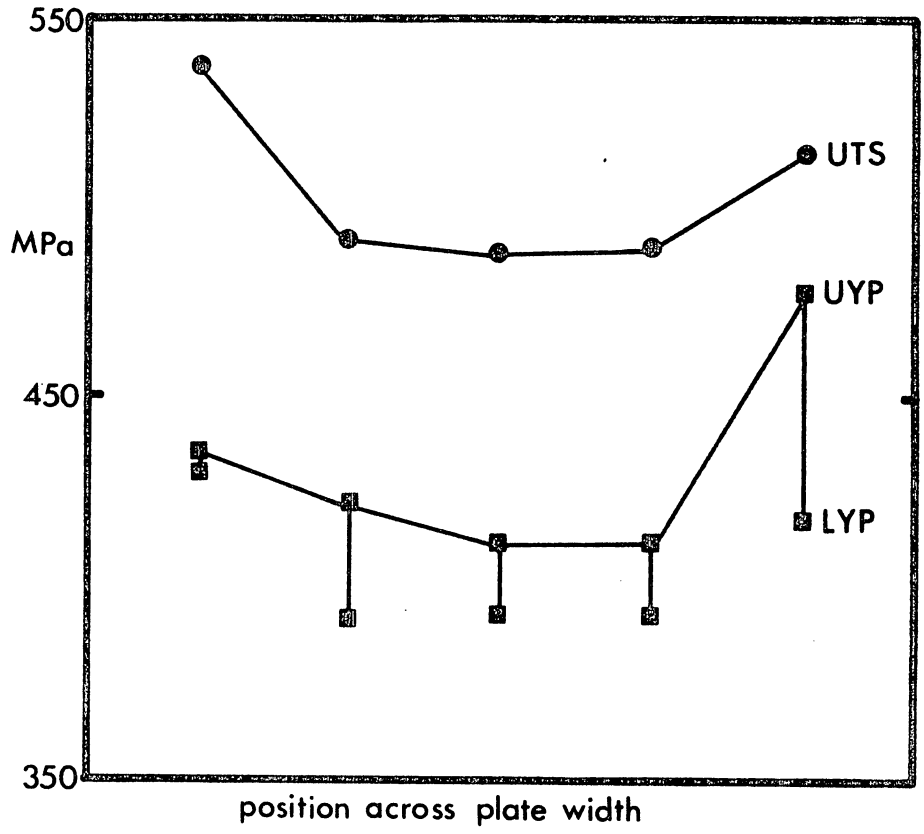

Figure 4.4 The variation of the tensile properties across the plate width.

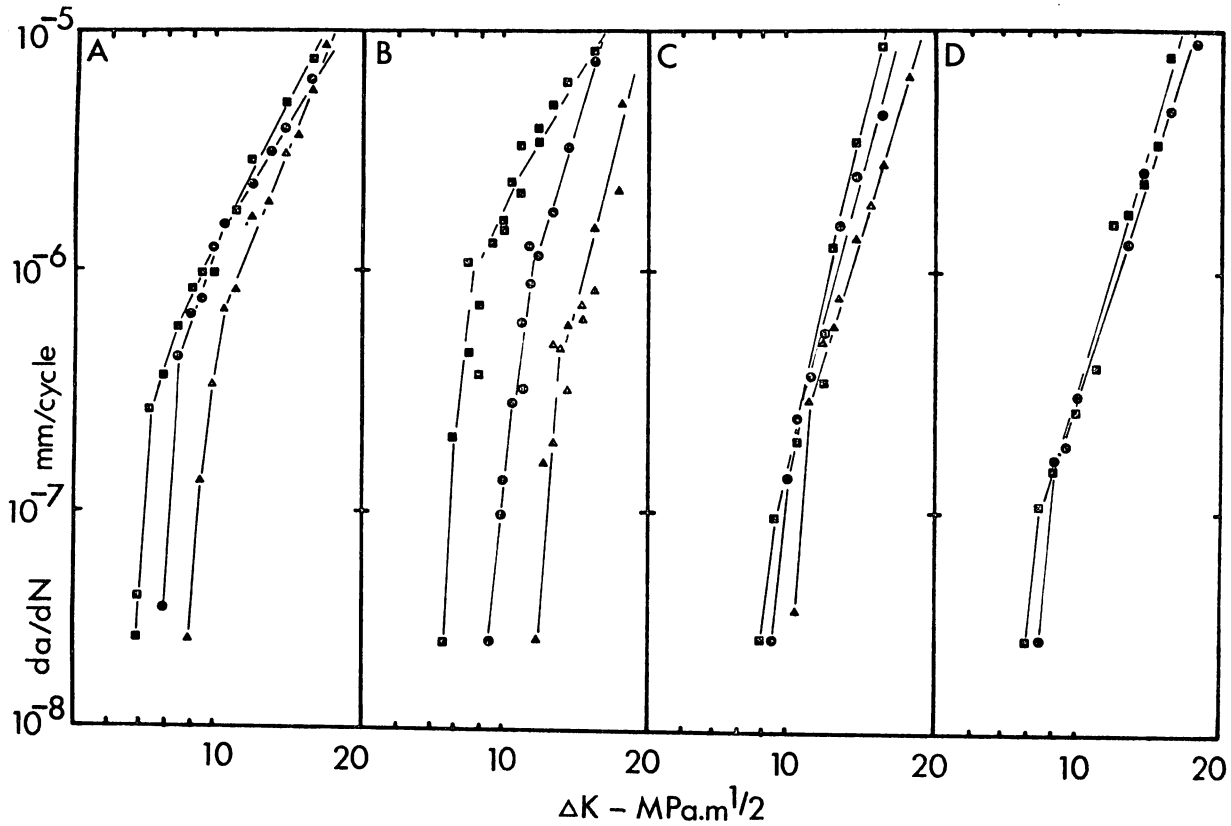

Figure 4.5 Fatigue crack growth curves for Fe-Ti-C.
a) as received, b) transformed at 800°C,
c) transformed at 725°C, d) transformed at 600°C.

▲ R = 0.1

● R = 0.3

■ R = 0.5

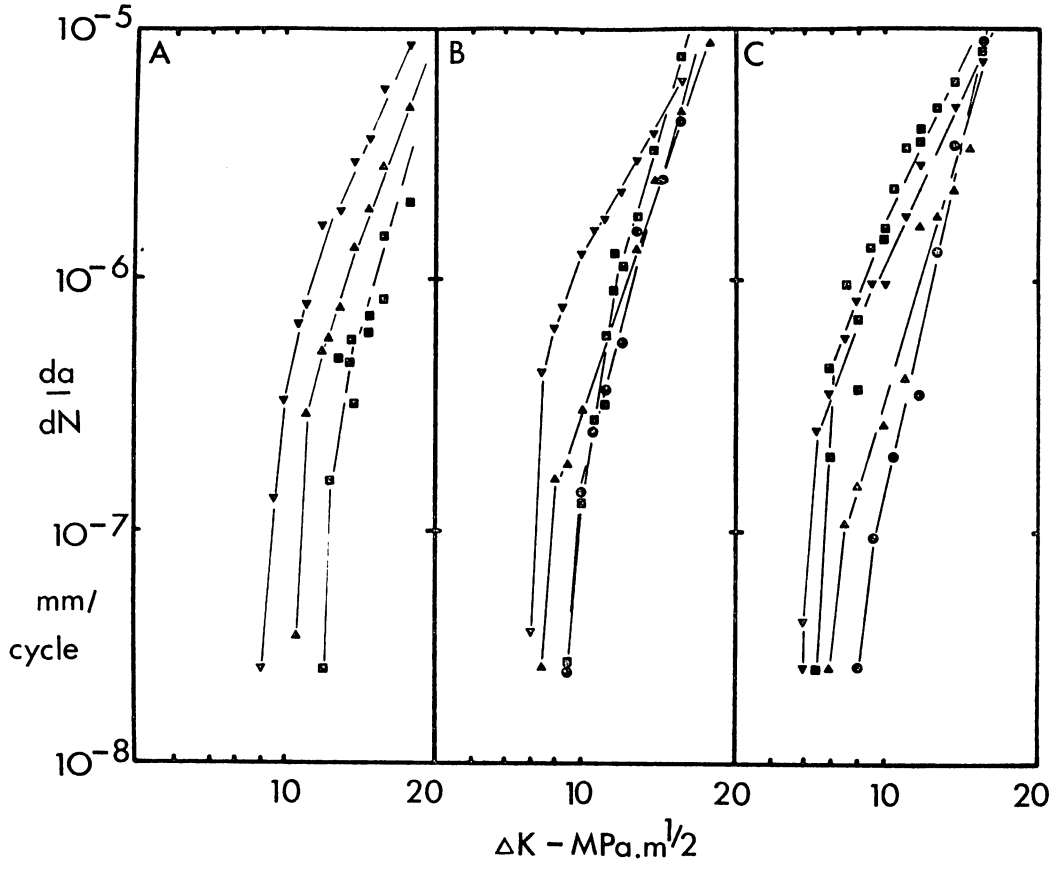

Figure 4.6 Fatigue crack growth curves for Fe-Ti-C.
a) R = 0.1, b) R = 0.3, c) R = 0.5.

▼ as received

■ transformed at 800°C

● transformed at 725°C

▲ transformed at 600°C

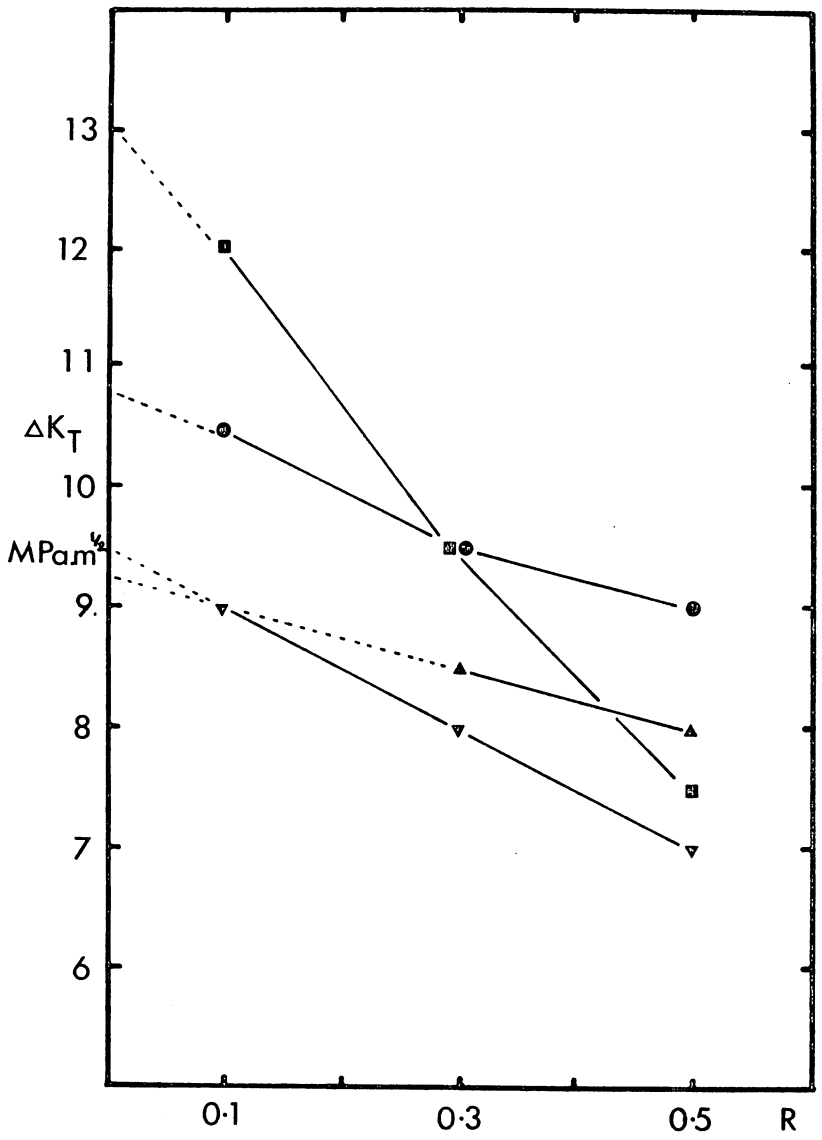

Figure 4.7 Graph of threshold value (ΔK_T) as a function of load ratio (R) and microstructure.

	σ_y	γ
▼ as received	411	0.4
■ 800°C	368	0.8
● 725°C	581	0.3
▲ 600°C	681	0.2

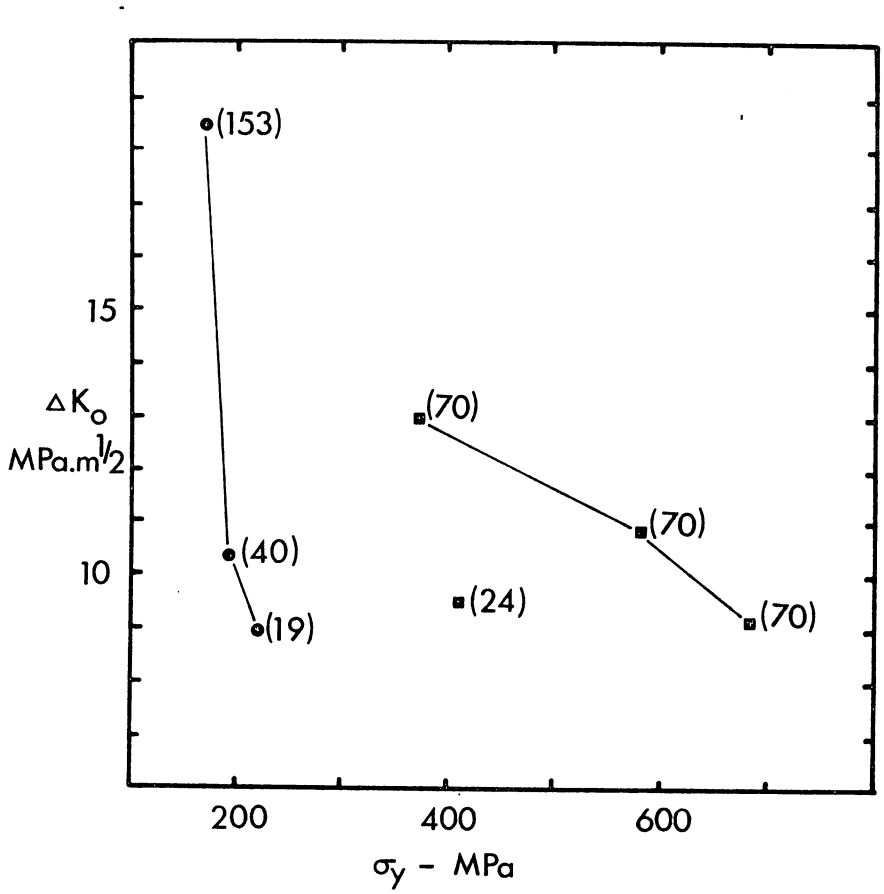

Figure 4.8 Graph of threshold value at R = 0 (ΔK_0) versus yield stress.

■ this work

● reference 56

( ) grain size in μm.

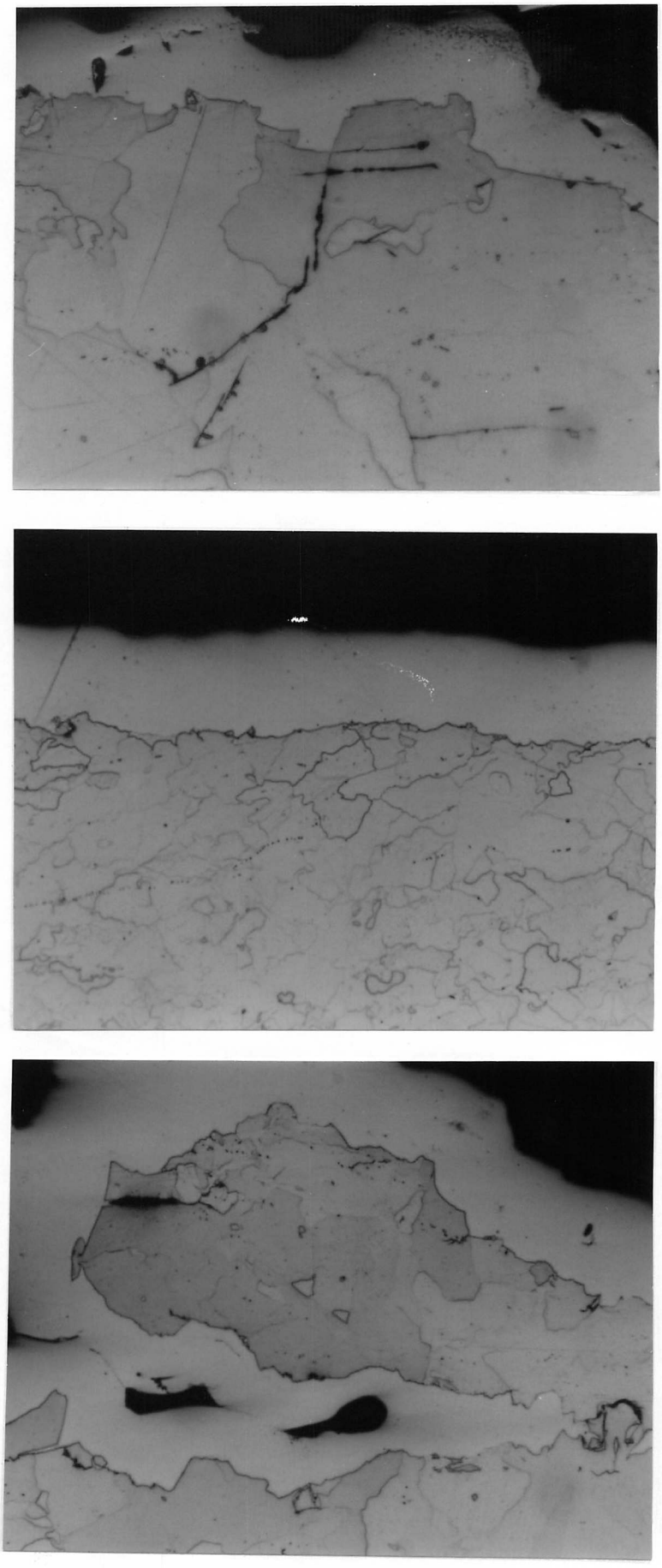

Figure 4.9 Nickel plated sections of fracture surfaces in the threshold region : a) transformed at 600°C ($\Delta K \sim 9.5$ MPa.$m^{\frac{1}{2}}$; R = 0.5), b) as received ($\Delta K \sim 7.0$ MPa.$m^{\frac{1}{2}}$; R = 0.5), c) transformed at 600°C ($\Delta K \sim 8.5$ MPa.$m^{\frac{1}{2}}$; R = 0.3) (x230).

CHAPTER FIVE.

TEMPER EMBRITTLEMENT DUE TO PHOSPHOROUS AND ANTINOMY IN STEELS STRENGTHENED BY INTERPHASE PRECIPITATION.

Introduction.

Many commercial steels undergo a progressive loss of toughness when cooled slowly through or held in the temperature range 350-550°C, and this is known as temper embrittlement. As the embrittling treatment is continued the impact transition temperature is increased and the upper shelf energy is decreased, this being associated with an increasing proportion of intergranular fracture. Most of the commercial materials which are susceptible to temper embrittlement are used in the quenched and tempered condition, and little work has been carried out on other microstructures. Since part of the interest in steels strengthened by interphase precipitation is directed towards replacing some of the more conventional quenched and tempered materials it is of interest to study how these precipitation hardened ferritic microstructures respond to heat treatments which would produce significant embrittlement in tempered martensite.

Temper embrittlement is caused by segregation of impurity elements to grain boundaries, thereby reducing the grain boundary cohesion (77). The principle impurity elements which are of importance in iron are :-

IV B	Si, Ge, Sn
V B	N, P, As, Sb, Bi
VI B	S, Se, Te

The group VI B impurities S, Se, and Te are probably the

most potent embrittling species in iron (78,79), but their strong affinity for manganese and chromium reduces their effective concentration to low levels. The impurities from groups IV B and V B are less potent embrittling species (77) but because they co-segregate to boundaries with other alloying elements such as nickel and manganese (80,81) their embrittling effect can be greater than that of the elements in group VI B. Hondros et al. (82) have shown that, for commercial steels produced in the United Kingdom, phosphorous is the most important embrittling impurity, followed by tin. Antimony and arsenic are much less important.

With the development of Auger electron spectroscopy (83) it has become possible to analyse intergranular fracture surfaces for the presence of impurity atoms. It is now clear that the change in impact transition temperature due to temper embrittling heat treatments can be directly related to the amount of impurity segregated to the grain boundary and to the potency of that segregated species in reducing intergranular cohesion (84-87). The degree of embrittlement is increased when the prior austenite grain size is increased (88,89) or when the material yield strength is increased (90-92).

Guttmann (81) put forward a thermodynamic argument which successfully rationalises the observed co-segregation effects of impurities and alloying elements. It has been shown, using Auger electron spectroscopy, that the grain boundary concentrations of alloying element and impurity are directly proportional in the systems Ni-Sb, Ni-P,

Ni-Sn (84,85,90) and Mn-Sb (81). The segregation in Ni-Cr steels can be far greater than that in Ni or Cr steels (90,93).

Very few workers have examined the influence of microstructure on susceptibility to temper embrittlement. Ouchi et al. (89) showed that a 0.15C-1.2Mn steel with a lower bainite microstructure was more susceptible to temper embrittlement than the same steel heat treated to give a mixed ferrite/bainite microstructure. Ohtani and McMahon (94) presented evidence that the fracture of prior austenite grain boundaries was not an essential feature of temper embrittlement. They showed that intergranular failure due to impurity segregation could occur along the boundaries of blocky ferrite and upper bainite, or on the boundaries of equiaxed ferrite produced by recrystallisation below the eutectoid temperature. If the prior austenite grain boundaries are sufficiently well preserved during the transformation of austenite to ferrite then these boundaries can still fracture after embrittling heat treatments. There is some evidence that some phosphorous segregation to grain boundaries in austenite can occur, although antimony does not segregate under these conditions. The same workers showed (84) that in a 3.5Ni-1.7Cr-0.008C-700ppmSb steel embrittlement in the recrystallised condition was analogous to that in the quenched and tempered condition, although the kinetics of segregation were much slower.

Experimental details.

The compositions of the alloys are given in Table 5.1.

Alloy G1 was supplied by the British Steel Corporation as 12.5mm. diameter hot rolled bar. Alloy G2 was prepared by remelting 2kg. of alloy G1 in a Viavac induction furnace and making an antimony addition a few minutes before casting. The $\frac{1}{2}$Cr-$\frac{1}{2}$Mo-$\frac{1}{4}$V steel was used for the fatigue tests in chapter 3, and a 2kg. melt with a ferro-phosphorous addition was made for alloy C2. The alloys were hot rolled and swaged to give rod for the tensile and impact specimen blanks. Heat treatments were carried out in tube furnaces with an argon atmosphere, salt baths and sealed in silica in a muffle for the embrittling treatments. The tensile specimen design was Hounsfield no.11. The impact specimens for alloys G1 and G2 were of the same design as those used for alloys F1-F3 in chapter 2, i.e. 6mm. diameter with a 1.2mm. notch depth. For alloys C1 and C2 the triple notched design shown in figure 5.1 was used. The specimen is fitted with specially machined sleeves so that three tests can be carried out on each specimen. It was found that deformation of the sleeves made some of the impact energy values questionable, although the fracture appearance transition curves were reliable.

Experimental results.

1. Embrittlement of Fe-1V-0.2C by antimony.

All the specimens were given a pre-treatment of 30 minutes at 1200°C and water quenched before austenitising for 15 minutes at 1150°C. The specimens were then either isothermally transformed for 10 minutes at 750°C and air cooled, or water quenched then tempered for 10 minutes at

Table 5.1 Compositions of the alloys tested.

	C	V	Cr	Mo	Sb	P
G1	0.25	1.06			<0.001	
G2	0.21	1.06			0.032	
C1	0.11	0.24	0.41	0.55		0.008
C2	0.15	0.29	0.38	0.56		0.056

Table 5.2 Summary of the results for the embrittlement of Fe-1V-0.2C.

		embrittled	
FATT (°C)	unembrittled		de-embrittled
G1 transformed at 750°C	195	195	195
quenched and tempered	70	80	90
G2 transformed at 750°C	200	170	170
quenched and tempered	100	155	85
σ_y (MPa)			
G1 transformed at 750°C	781	860	692
quenched and tempered	1287	1342	1338
G2 transformed at 750°C	764	714	709
quenched and tempered	1177	1187	1178

750°C and air cooled. The embrittling treatment was 24 hours at 550°C followed by water quenching, and some specimens were given a de-embrittling treatment of 30 minutes at 650°C and water quenched. The fracture appearance transition curves are presented in figures 5.2 and 5.3 and summarised in Table 5.2 which also includes the yield strengths given by each heat treatment. For the pure alloy (G1) the fracture appearance transition temperature in both the isothermally transformed and the quenched and tempered microstructures is unaffected by the embrittling and de-embrittling heat treatments. The fracture appearance transition temperature is higher for isothermally transformed than for quenched and tempered specimens, despite the higher yield stresses of the latter. In the antimony doped alloy (G2) there is a slight decrease in the impact transition temperature when isothermally transformed specimens are given embrittling or de-embrittling heat treatments. In contrast, for quenched and tempered specimens, the embrittling heat treatment increases the impact transition temperature by 55°C. The de-embrittling treatment reduces the impact transition temperature to below that of the unembrittled condition.

The pure alloy is not sensitive to temper embrittlement in this temperature range, although there is significant embrittlement in the impure alloy in the martensitic condition. The isothermally transformed specimens do not embrittle when given heat treatments that produce significant embrittlement in martensitic specimens.

2. Embrittlement of $\frac{1}{2}$Cr-$\frac{1}{2}$Mo-$\frac{1}{4}$V steel by phosphorous.

The specimens were austenitised for 15 minutes at 1100°C and then either isothermally transformed for 30 minutes at 675°C and water quenched, or water quenched and then tempered for 30 or 60 minutes at 650°C and water quenched. Specimens were embrittled for either 10 or 100 hours at 500°C and water quenched. The fracture appearance transition temperatures and yield strengths are given in Table 5.3. In the quenched and tempered condition both alloys are subject to temper embrittlement, the embrittlement being both more rapid and more significant in the high phosphorous alloy C2. The commercial phosphorous level is sufficient to give measurable embrittlement. In the isothermally transformed condition the results are more ambiguous. The change in fracture appearance transition temperature is greater in the commercial purity material than in that with the higher phosphorous level. The reasons for this are not clear, but it can be seen that the embrittlement in the high phosphorous material in the isothermally transformed condition is less than that for the quenched and tempered condition.

Discussion.

It has been shown (Table 5.2) for Fe-1V-0.2C doped with antimony that temper embrittlement occurs in tempered martensite, but not in the isothermally transformed ferrite. There are a number of possible reasons for this. Firstly, the yield strength of the isothermally transformed ferrite is significantly less than that of

Table 5.3 Fracture appearance transition temperatures and yield strengths in alloys C1 and C2.

FATT (°C)	unembrittled	10 hours 500°C	100 hours 500°C
C1 tempered 30/650	40	45 (+5)	80 (+40)
tempered 60/650	50	55 (+5)	85 (+35)
transformed 30/675	160	195 (+35)	225 (+65)
C2 tempered 30/650	55	155 (+100)	190 (+135)
tempered 60/650	50	150 (+100)	180 (+130)
transformed 30/675	165	185 (+20)	180 (+15)

Yield strength for alloy C1 (MPa)			
tempered 30/650	1163	1157	1140
tempered 60/650	1131	1092	1109
transformed 30/675	887	862	897

the tempered martensite. Many workers (90-92) have shown that the degree of temper embrittlement is increased as the yield strength is increased, and the apparent absence of temper embrittlement in the ferritic condition may be due entirely to the lower yield strength. It has also be shown (91) that as the yield strength is decreased a higher impurity level is required to produce embrittlement effects. Secondly, there is some evidence (84) that the kinetics of segregation of impurities in ferrite may be slower than for their segregation in tempered martensite. Figure 5.4 illustrates a further reason for the decreased susceptibility of the ferritic microstructures to temper embrittlement. The poor cleavage resistance of isothermally transformed ferrite strengthened by interphase precipitation of vanadium carbide has been dealt with in chapter 2, and it is clear that a far greater reduction in the intergranular fracture stress is necessary in the ferritic than the martensitic condition if the intergranular fracture stress is to be reduced to below the cleavage stress. The apparent absence of temper embrittlement in ferrite may therefore be due more to the inherently poor fracture resistance of the ferrite than to any reduction in the susceptibility to antimony segregation.

In the commercial purity $\frac{1}{2}$Cr-$\frac{1}{2}$Mo-$\frac{1}{4}$V steel the phosphorous level (0.008%) was sufficient to give significant embrittlement in the martensitic condition, the embrittlement being greatly increased by increasing the phosphorous level to 0.056%. The results for the isothermally condition are more ambiguous, but the embrittlement appears to be less pronounced. The arguments set out above for Fe-1V-0.2C

concerning the effects of strength level, slower segregation in ferrite and the low cleavage strength of the ferrite will also apply to the $\frac{1}{2}$Cr-$\frac{1}{2}$Mo-$\frac{1}{4}$V steels. The greater embrittlement in the martensitic condition is not too important commercially, since this material cannot be water quenched to a fully martensitic microstructure in thicknesses much greater than 10mm., and it is usually used in the normalised or bainitic condition.

Some workers have examined the effects of alloying elements on susceptibility to temper embrittlement. Narayan and Murphy (95) showed that molybdenum had a beneficial effect, this effect being enhanced by the presence of vanadium. This enhancement of the scavenging effect in the presence of vanadium is probably because vanadium, being a stronger carbide former than molybdenum, would precipitate preferentially, thereby increasing the extent of molybdenum solid solution. Other workers (89,96) have presented further evidence that molybdenum has a beneficial effect, although this scavenging effect of molybdenum ceases if the molybdenum is precipitated as a carbide (96,97). Molybdenum in solid solution inhibits the diffusion of phosphorous (89,96). In the $\frac{1}{2}$Cr-$\frac{1}{2}$Mo-$\frac{1}{4}$V steel used here most of the molybdenum and vanadium would be precipitated as carbide, and the 100^{o}C rise in impact transition temperature for the impure alloy in the martensitic condition suggests that these alloying elements have not had a significant scavenging effect in this material.

Conclusions.

From a study of temper embrittlement in an Fe-1V-0.2C steel doped with antimony it is concluded that :

1. there is significant embrittlement of the impure alloy in the martensitic condition after holding at 550°C, this embrittlement being removed by a 650°C heat treatment.

2. there is no significant embrittlement of the impure alloy in the ferritic condition.

3. the difference between the martensitic and ferritic conditions is attributed to a combination of the lower yield strength of the ferrite, slower segregation kinetics and the low cleavage strength of the ferrite.

From a study of the effects of phosphorous on a $\frac{1}{2}$Cr-$\frac{1}{2}$Mo-$\frac{1}{4}$V steel it is concluded that :

4. the commercial phosphorous level is sufficient to produce significant embrittlement.

5. embrittlement of the impure alloy is greater for the martensitic than for the ferritic condition.

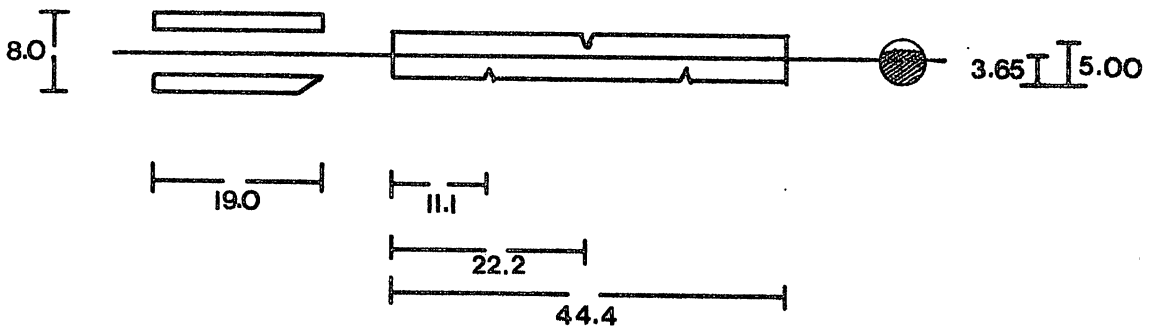

Figure 5.1 Design of impact specimens for embrittlement studies in $\frac{1}{2}$Cr-$\frac{1}{2}$Mo-$\frac{1}{4}$V steel.

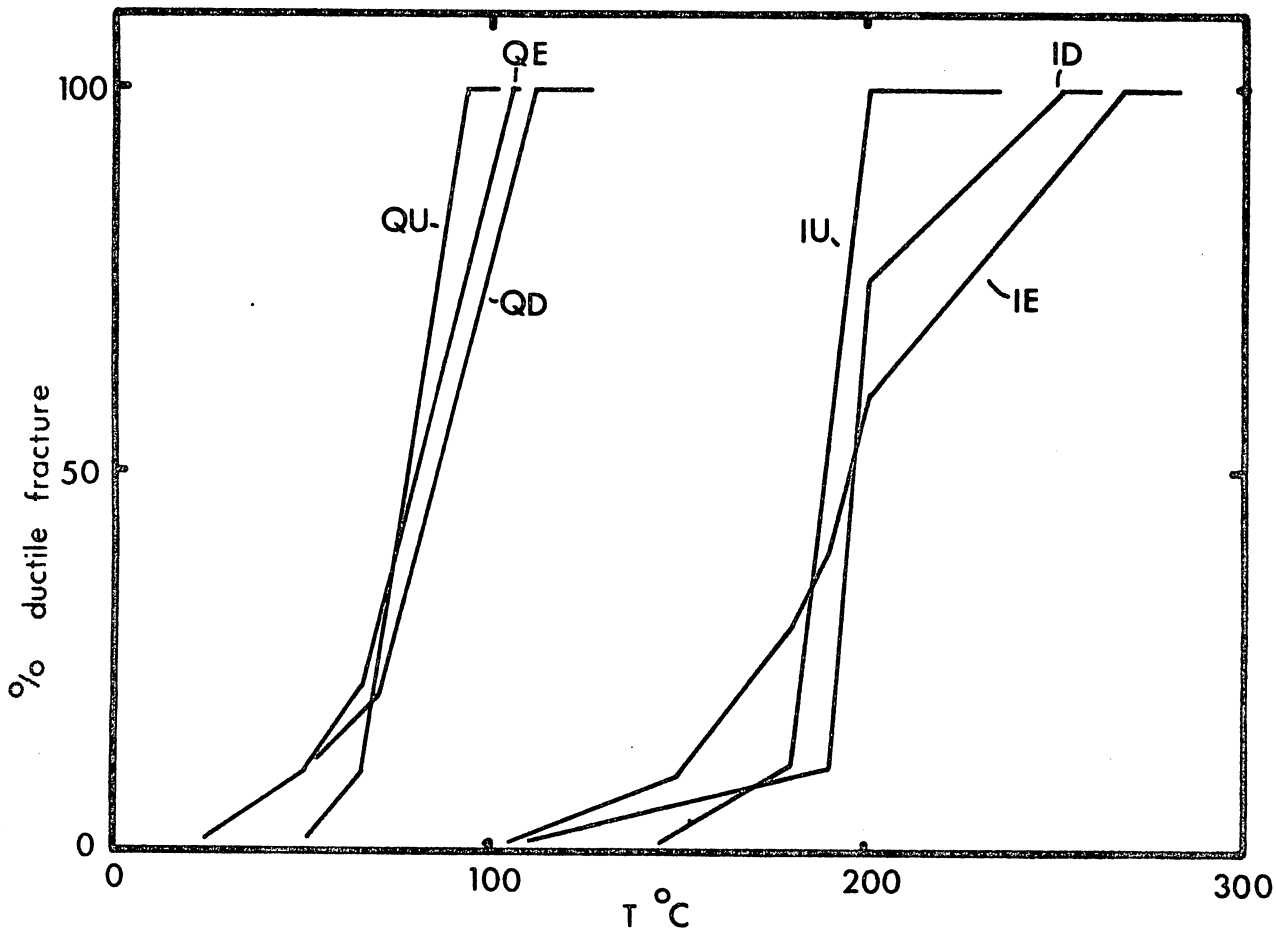

Figure 5.2 Ductile-brittle transition curves for alloy G1.

QU - quenched and tempered, unembrittled

QE - quenched and tempered, embrittled

QD - quenched and tempered, de-embrittled

IU - isothermally transformed, unembrittled

IE - isothermally transformed, embrittled

ID - isothermally transformed, de-embrittled

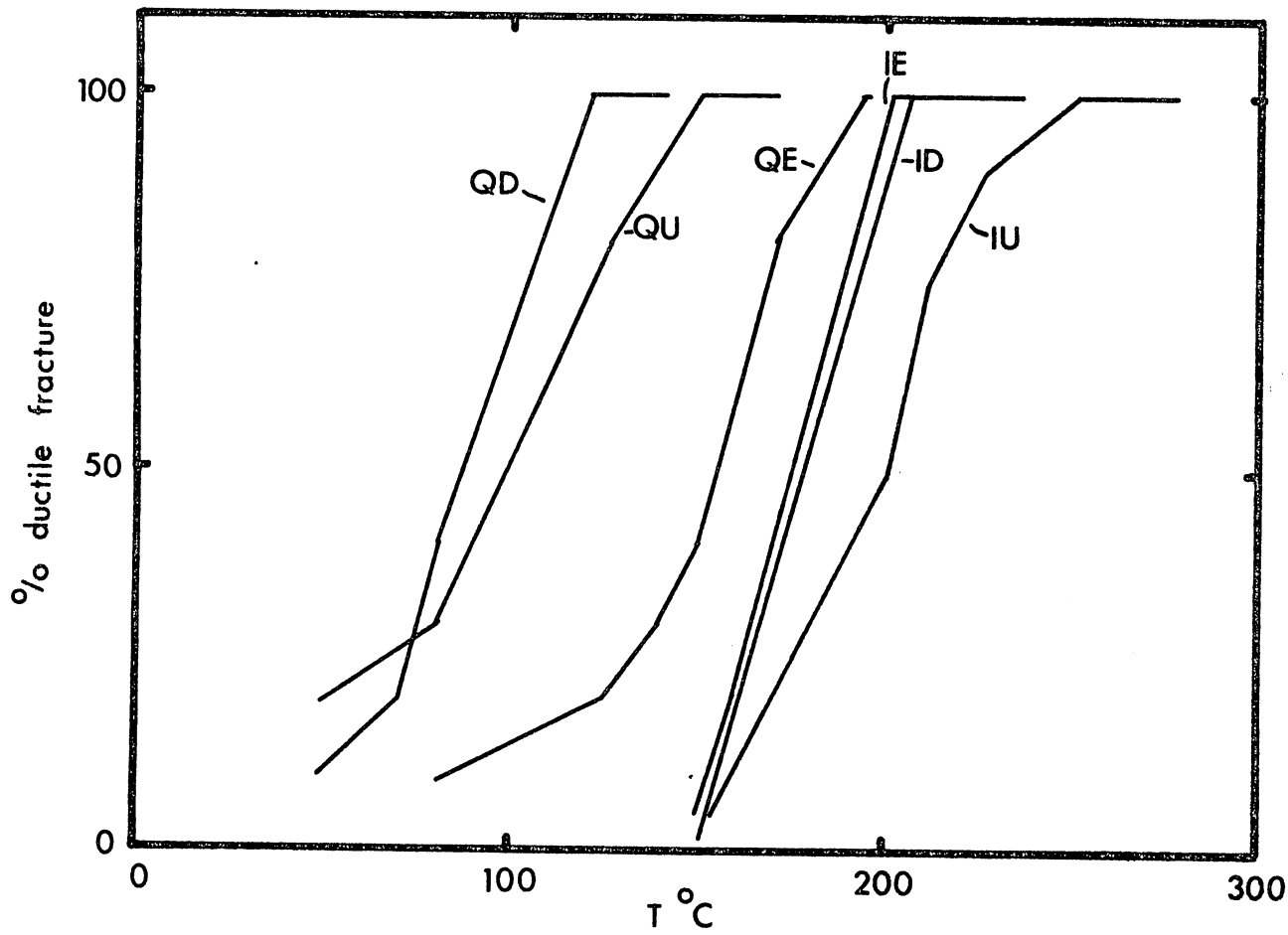

Figure 5.3 Ductile-brittle transition curves for alloy G2.
(the key is given with figure 5.2)

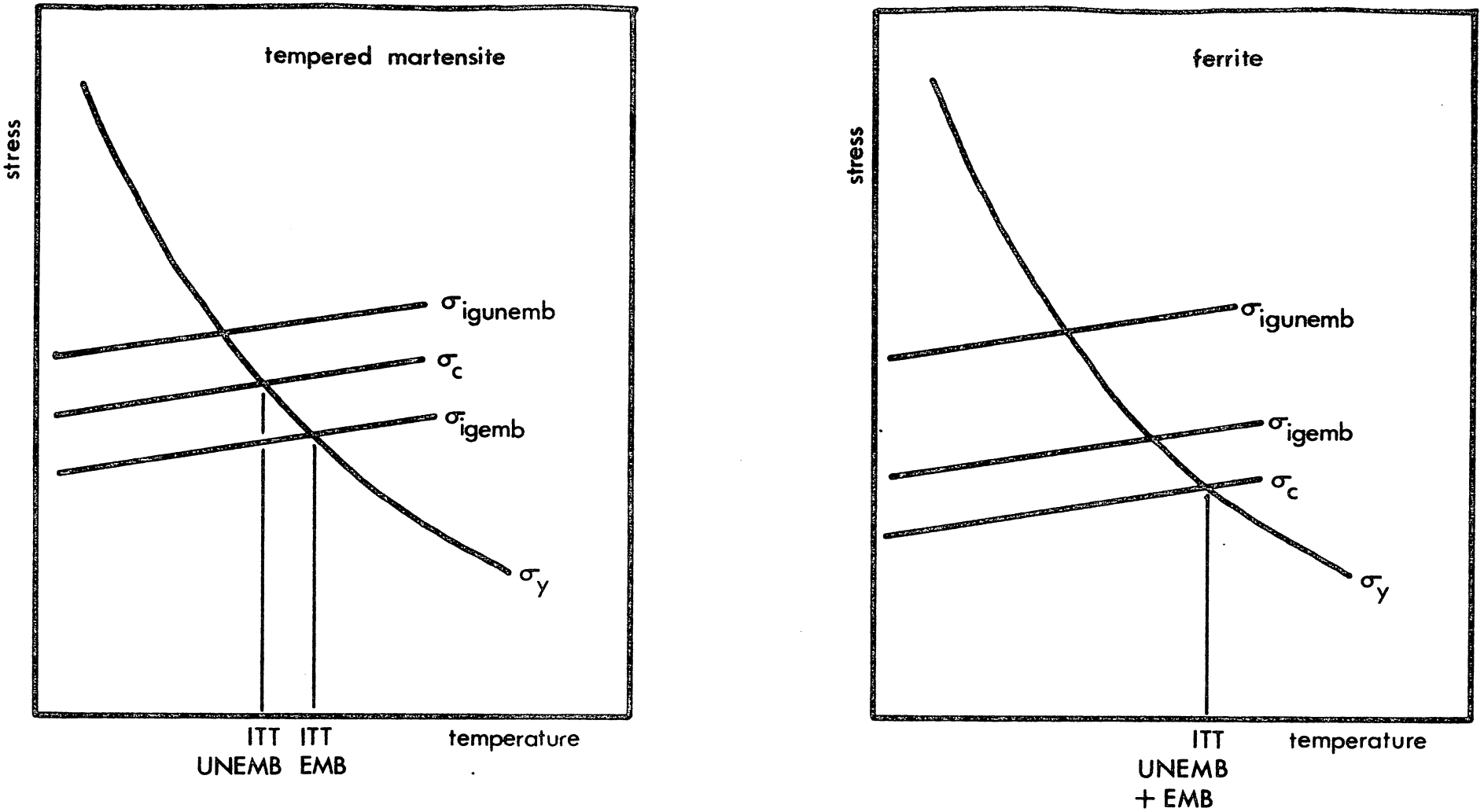

Figure 5.4 Schematic diagram of the effect of embrittling heat treatments on different microstructures.

σ_y - yield stress σ_c - cleavage stress

$\sigma_{igunemb}$ - intergranular fracture stress without embrittlement

σ_{igemb} - intergranular fracture stress with embrittlement

CHAPTER SIX.

CONCLUDING DISCUSSION AND SUGGESTIONS FOR FURTHER WORK.

Introduction.

High strength steels are being used to an increasing extent. Their evolution has been largely empirical and this has resulted in many expensive alloying elements being used inefficiently. Most of these steels are used in the quenched and tempered condition, and this can give problems of quench cracking and temper embrittlement. Isothermal transformation from austenite to ferrite in various low alloy steels gives a high strength precipitation hardened ferritic microstructure which avoids quench cracking problems.

For a high strength steel to be used commercially it must have a range of good properties, not just high strength. Extremely high strength steels are not difficult to produce, but to produce a steel with both high strength and high toughness is particularly difficult. The steel may also need to have good fatigue and creep properties, good weldability and high corrosion resistance. This chapter summarises what is known about the mechanical properties of steels strengthened by interphase precipitation and gives an assessment of their possible commercial significance. The end of the chapter contains some suggestions for further work.

Summary of the mechanical properties of steels strengthened by interphase precipitation.

1. Tensile properties.

The tensile properties of steels strengthened by

interphase precipitation are controlled by the isothermal transformation temperature (or the rate of cooling through the transformation range), the volume fraction of carbides in ferrite and the reaction kinetics. As the isothermal transformation temperature is reduced (18,20,98,99) the strength of the material is increased, and increasing the rate of cooling through the transformation range also increases the resulting strength level (18,19). The strength level is increased by increasing the carbide volume fraction (20,98) or by accelerating the kinetics of the transformation (18,20).

The yield strength (σ_y) data can be analysed using a modified Hall-Petch equation (100) :

$$\sigma_y = \sigma_o + \sigma_{ss} + k_y d^{-\frac{1}{2}} + \sigma_p$$

where σ_o is the inherent matrix friction stress, σ_{ss} the solis solution hardening contribution to the yield stress, d is the grain size, k_y a constant and σ_p the precipitation hardening contribution to the yield stress. Various workers have extracted σ_p from their results and investigated the dependence of σ_p on the precipitate sheet spacing (λ). It is found that the data fit an equation of the form :

$$\sigma_p = k\lambda^{-n}$$

where k and n are constants. Typical values of n for a range of steels strengthened by interphase precipitation of vanadium carbide are :

Batte et al. (98)	0.5
Batte and Honeycombe (20)	0.7
Edmonds (19)	1.1
Wilyman (18)	0.45

The first value of 0.5 can be ignored because the same results appear to have been recalculated to give n=0.7 (20). Each of these workers attempted to apply existing precipitation hardening theories to the non-random carbide dispersion produced by interphase precipitation. It has frequently been shown (7, 19, 98, 101) that in coarse dispersions resulting from interphase precipitation the dislocations bow around the precipitates rather than cutting them, and some tentative calculations suggset that the vanadium carbide platelets are too large to be cut by dislocations (8). Wilyman (18) noted that the exponent n appeared to be dependent on the intersheet spacing λ. Edmonds (19) examined coarse dispersions resulting from controlled cooling from austenite to obtain n=1.1, although he noted that it was difficult to attach much significance to the result because of the range of intersheet spacings that results from controlled cooling. Batte and Honeycombe (20) investigated finer precipitate dispersions resulting from isothermal transformation in the range 725-800°C to give n=0.7, and Wilyman (18) obtained n=0.45 from even finer dispersions from transformation in the range 650-700°C. It appears that n is reduced as λ is reduced. Wilyman suggested that at large intersheet spacings the dislocations bow around the precipitates, but that at very fine spacings some particle cutting occurs, so that n is reduced. This is in agreement with the results of Scarlin and Edington (102) who showed that vanadium carbides of 3.5nm. diameter could be cut by dislocations.

It has been observed (98) that these isothermally

transformed ferritic microstructures have a high initial work hardenening rate, although this reduces to that of pure iron after 10% plastic strain. The ductility is greatly reduced as the yield strength is increased (98), and Dulieu et al. (103) suggest that this precipitation strengthening mechanism can only be used commercially for yield strengths up to 600MPa if there is to be adequate ductility.

2. Toughness and impact properties.

Dulieu et al. (103) investigated a series of Fe-V-C alloys in an attempt to develop practicable low alloy steels exploiting interphase precipitation mechanisms. They found that these alloys had poor room temperature impact properties, and they attributed this to the large austenite grain size that resulted from the high austenitisation temperature needed for complete carbide solution, the high yield strength of the ferrite in relation to its grain size and the presence of coarse carbide particles on grain boundaries. Freeman (21) studied the room temperature COD of several Fe-Ti-C steels in the ferritic and martensitic condition. He showed that the COD values were very similar, although since these values are all low it would appear that most of the specimens failed in a brittle manner. In chapter 2 of this report information is presented on the variation of impact transition temperature with yield strength in a series of Fe-V-C alloys. It is shown that the impact transition temperature is increased by 0.54-0.64°C for each 1 MPa increase in yield strength by precipitation hardening, the rate of increase being comparable for the

non-random interphase precipitation dispersion and a more random aged dispersion. The non-random precipitate dispersion can modify the path of a cleavage crack through the microstructure under certain conditions, but this appears to be a secondary effect. The low toughness of the isothermally transformed ferritic microstructures can thus be attributed primarily to the high matrix yield strength. The toughness will be improved by grain refinement (18).

3. Fatigue properties.

There are four areas in which the fatigue properties must be considered to ensure a balanced understanding of the fatigue properties of a material. The resistance of a material to the initiation of a fatigue crack is most easily assessed by S-N testing, the fatigue limit being a stress level below which propagating fatigue cracks are not formed. The fatigue crack growth properties need to be determined in the threshold region, the threshold being the stress intensity level at which a pre-existing fatigue crack ceases to propagate, in the intermediate growth rate range and at high crack growth rates leading up to final failure of the specimen.

Information on the S-N behaviour of these steels has been presented in reference 1 and chapter 3 of this report. In an Fe-1V-0.2C steel it was found that the fatigue limit was highest for a quenched and tempered microstructure, a ferritic microstructure of the same ultimate tensile strength giving a lower fatigue limit. The fatigue ratio, the ratio of the fatigue limit to the ultimate tensile strength, was reduced as the isothermal transformation temperature was

reduced. The fine grain size as received ferritic microstructure gave the highest fatigue ratio. In a $\frac{1}{2}$Cr-$\frac{1}{2}$Mo-$\frac{1}{4}$V steel a quenched and tempered microstructure gave a much higher fatigue ratio than isothermally transformed ferrite, despite the much higher strength level of the quenched and tempered material. The S-N behaviour of isothermally transformed ferritic materials appears to be inferior to that of tempered martensite at similar strength levels.

Results for the threshold region are given in reference 1 and in chapter 4 of this report. In the $\frac{1}{2}$Cr-$\frac{1}{2}$Mo-$\frac{1}{4}$V steel it was shown that the large grain size low yield strength ferrite microstructures gave the highest threshold values, the thresholds being lower for bainites and tempered martensite with higher yield strengths. Tempered martensite gave a low threshold and a high fatigue limit, whereas precipitation hardened ferrite gave a high threshold and a low fatigue limit. This indicates the conflicting requirements for resistance to fatigue crack initiation and to fatigue crack growth in steels. Thresholds were determined in an Fe-Ti-C steel over a range of ferrite grain sizes and yield strengths, the yield strength being varied by changing the isothermal transformation temperature. The threshold value is reduced by increasing the yield strength or by reducing the grain size. The threshold values of isothermally transformed ferritic microstructures are superior to those of tempered martensite, but this may be attributed to the lower yield strength and larger grain size of the former.

In the intermediate fatigue crack growth rate range the properties of ferrite strengthened by interphase

precipitation are very similar to those of tempered martensite or bainite (1). The isolated incidence of a cleavage static mode of failure in association with normal fatigue crack growth in the ferritic material may give a slight increase in the fatigue crack growth rate at higher stress intensity levels.

In the high fatigue crack growth rate range the properties of isothermally transformed ferrite are inferior to those of bainite or tempered martensite (1). At these high stress intensity levels, which can exceed K_{IC}, the toughness of the material determines the fatigue crack growth rate. Low toughness materials fail at a much lower ΔK than those of high toughness, and the fatigue results at these high stress intensity values illustrate again the low toughness of the isothermally transformed ferritic microstructures.

It can thus be seen that if the fatigue properties of isothermally transformed ferrite and tempered martensite are compared then their properties are comparable in the intermediate fatigue crack growth rate range, the ferrite is superior in the threshold region, and the martensite has superior resistance to fatigue crack initiation and to final unstable crack propagation.

4. Creep properties.

The creep properties of isothermally transformed ferrite have been compared with those of tempered martensite or bainite in a $\frac{1}{2}$Cr-$\frac{1}{2}$Mo-$\frac{1}{4}$V steel and an Fe-1V-0.2C model system (104-106). It was found that primary creep was more extensive in isothermally transformed ferrite than in the other microstructures. The maximum secondary creep strength and

creep rupture strength were given by microstructures produced by transformation from $\gamma \rightarrow \alpha$ close to the bay in the TTT curve. Creep fracture occurred along prior austenite grain boundaries in bainite or martensite and along ferrite boundaries in the ferrite. The isothermally transformed ferrite therefore had a smaller effective grain size with respect to the fracture process, and this was reflected in the greater creep ductility.

Overall assessment of the mechanical properties of steels strengthened by interphase precipitation.

As has been stated previously, any steel which is to be used commercially must have an attractive combination of properties, not just high strength. The most important combination is that of strength and toughness. It is possible to achieve high strength levels by interphase precipitation of vanadium or titanium carbide, but this is associated with a drastic reduction in toughness. The only way to increase strength and toughness simultaneously is to refine the grain size. Gladman et al. (107) state that for silicon killed C-Mn steels with some vanadium and niobium additions it is possible to obtain a relationship of the form :

$$ITT\ (^{o}C) = \text{constant} - 11.5\ d^{-\frac{1}{2}}$$

where d is the ferrite grain size in mm.. Including a term for the effects of precipitation strengthening gives :

$$ITT\ (^{o}C) = \text{constant} - 11.5\ d^{-\frac{1}{2}} + (ITT)_{p}$$

Table 6.1 contains values for the reduction in impact transition temperature that would be expected from reducing

the ferrite grain size from 20 μm.. In figure 2.2 a yield stress of 750 MPa gives an impact transition temperature of 200°C. To reduce this temperature to a commercially acceptable level by grain refinement would require a 1 μm. ferrite grain size which is beyond the capacity of any existing grain refinement procedure. A reduction to a 5 μm. ferrite grain size would only lower the impact transition temperature to 120°C.

The fatigue properties of steels strengthened by interphase precipitation are either equivalent to, better than or worse than the properties of more conventional steels, depending on which aspect of fatigue failure is considered. Much the same is true of the creep properties of steels strengthened by interphase precipitation. It is therefore the low toughness and high impact transition temperatures of the isothermally transformed ferritic materials that constitute the major obstacle to their consideration for commercial use at medium and high strength levels. Interphase precipitation does provide a valuable strength increment in many low alloy controlled rolled steels, and several firms have produced practicable steels of up to 550 MPa yield strength (108). Dulieu et al. (103) considered that 600 MPa could be a practical upper limit where the yield strength was increased by precipitation hardening.

Suggestions for further work.

1. In chapter 4 it was shown that microstructure, mechanical properties and environment each have a very significant effect on the threshold for fatigue crack growth.

Table 6.1 Reduction in the impact transition temperature as the grain size is reduced from 20 μm.

d(μm)	$d^{-\frac{1}{2}}$(mm)	$11.5d^{-\frac{1}{2}}$	ITT(°C)
20	7.07	81.3	0
10	10.0	115	34
5	14.1	163	82
2	22.4	257	176
1	31.6	364	283
0.5	44.7	514	433
0.2	70.7	813	732
0.1	100	1150	1069

A hydrogen embrittlement model can be used to explain many features of the threshold fatigue behaviour of steels, and it would be useful to be able to separate the mechanical and environmental contributions to the threshold behaviour to facilitate firstly a more complete understanding of the threshold region and secondly the design of steels with high threshold values.

It would be comparatively easy to construct an environmental chamber for a Mand servohydraulic testing machine, such that threshold fatigue tests could be carried out in normal air, high vacuum or any controlled atmosphere. This rig could then be used to measure threshold values, and crack growth rates in the threshold region, as a function of :

1. environment
2. material yield strength
3. microstructure
4. size of the microstructural unit (grain size etc.)
5. material composition
6. load ratio
7. testing frequency

A comprehensive series of tests such as these would provide a fairly complete characterisation of the threshold region.

2. The iron plating technique for fine scale fractography can be used in many situations other than those examined here. Work is in hand to use this technique to examine white layers produced on steel surfaces, and it is hoped that this will lead to the solution of this particular problem. The technique has many experimental difficulties associated

with it, but further practise may resolve these difficulties.

3. It may be feasible to use selected area channelling pattern techniques on the scanning electron microscope to determine the cleavage planes of ferrite strengthened by interphase precipitation of vanadium carbide as a function of both the isothermal transformation temperature and the fracture temperature. There may be a problem of low angular resolution of the selected area channelling pattern after fracture at room temperature due to the large amount of dislocation motion that accompanies the passage of a cleavage crack under these conditions. The lattice distortion would be less severe after fracture at liquid nitrogen temperatures. It would be useful to know the cleavage plane distribution for Fe-1V-0.2C isothermally transformed at 790°C or 725°C, and fractured by impact at either room temperature or -196°C.

REFERENCES.

1. J.P.Benson Ph.D. thesis, University of Cambridge, 1976.
2. A.T.Davenport and R.W.K.Honeycombe Proc.Roy.Soc., A322,(1971),191.
3. P.R.Howell, J.V.Bee and R.W.K.Honeycombe to be published.
4. A.D.Batte and R.W.K.Honeycombe JISI,211,(1973),284.
5. J.P.Benson and D.V.Edmonds accepted for publication in Materials Science and Engineering.
6. T.Gladman JISI,203,(1965),1038.
7. J.P.Benson and D.V.Edmonds Proc.ICF4, Fracture 1977, vol. 2, p.65.
8. A.D.Batte Ph.D. thesis, University of Cambridge, 1971.
9. N.K.Balliger Ph.D. thesis, University of Cambridge, 1977.
10. U.H.Lindborg and B.L.Averbach Acta Met.,14,(1966),1583.
11. J.R.Low, J.F.Stein, A.M.Turkalo and R.P.Laforce Trans. AIME,242,(1968),14.
12. G.Knowles and P.M.Kelly ISI Special Report No. 145, (1971),9.
13. C.J.Simensen unpublished work, University of Cambridge, (1971).
14. E.Hornbogen Trans.ASM,57,(1964),120.
15. S.R.Goodman, S.S.Brenner and J.R.Low Met.Trans.,4,(1973), 2363 and 2371.
16. G.R.Speich "Precipitation from iron base alloys", (1963),66.
17. E.Hornbogen and R.C.Glenn Trans AIME,218,(1960),1064.
18. P.R.Wilyman Ph.D. thesis, University of Cambridge, 1976.
19. D.V.Edmonds Met.Trans.,4,(1973),2527.
20. A.D.Batte and R.W.K.Honeycombe Met.Sci.J.,7,(1973),160.
21. S.Freeman and R.W.K.Honeycombe Met.Sci.,11,(1977),59.
22. T.Gladman, B.Holmes and I.D.McIvor ISI Special Report

No.145,(1971),68.

23. W.B.Morrison JISI,201,(1963),317.

24. F.B.Pickering "Towards improved ductility and toughness", Climax Molybdenum publication,(1971),9.

25. N.P.Allen, B.E.Hopkins and J.E.McLennan Proc.Roy.Soc., A234,(1956),221.

26. R.O.Ritchie and J.F.Knott Proc.Conf. on Mechanics and Mechanisms of Crack Growth, Cambridge, (1973).

27. C.J.Beevers, R.J.Cooke, J.F.Knott and R.O.Ritchie Met. Sci.,9,(1975),119.

28. J.Weertman Int.J.Fract.Mech.,2,(1966),460.

29. J.Weertman Int.J.Fract.Mech.,5,(1969),13.

30. R.W.Lardner Phil.Mag.,17,(1967),71.

31. L.P.Pook and N.E.Frost Int.J.Fract.,9,(1973),53.

32. P.E.Irving and L.N.McCartney Met.Sci.,11,(1977),351.

33. T.C.Lindley and C.E.Richards Proc. BSC/ISI Conf. on Effects of second phase particles on the mechanical properties of steel, Scarborough, (1971).

34. T.W.Crooker and E.A.Lange Proc. Welding Institute Conf. on Fatigue of welded structures, Brighton, (1970).

35. C.E.Richards and T.C.Lindley Eng.Fract.Mech.,4,(1972),951.

36. K.R.Dowse and C.E.Richards Met.Trans.,2,(1971),599.

37. T.C.Lindley, C.E.Richards and R.O.Ritchie Proc. Conf. on Mechanics and Physics of fracture, Cambridge, (1975).

38. J.F.Throop and G.A.Miller ASTM STP No.467,(1970).

39. R.O.Ritchie and J.F.Knott Acta Met.,21,(1973),639.

40. R.O.Ritchie and J.F.Knott Mater.Sci.Eng.,14,(1974),7.

41. W.Elber Eng.Fract.Mech.,2,(1970),37.

42. T.C.Lindley and C.E.Richards Mat.Sci.Eng.,14,(1974),281.

43. P.E.Irving, J.L.Robinson and C.J.Beevers Eng.Fract. Mech.,7,(1975),619.

44. J.R.Griffiths and C.E.Richards Mat.Sci.Eng.,11,(1973),305.

45. D.J.F.Ewing and R.Hill J.Mech.Phys.Solids,15,(1967),115.

46. D.J.F.Ewing and C.E.Richards J.Mech.Phys.Solids, 22,(1974),27.

47. J.L.Swedlow Int.J.Fract.Mech.,5,(1969),33.

48. A.A.Wells Eng.Fract.Mech.,1,(1969),399.

49. T.Yokobori, I.Kawada and H.Hata Reports of the Research Institute for Strength and Fracture of Materials, Tohoku University, Sendai, Japan, 9,(1973),35.

50. E.H.Niccolls Scripta Met.,10,(1976),295.

51. L.N.McCartney and P.E.Irving Scripta Met.,11,(1977),181.

52. J-P.Bailon, J.Masounave and C.Bathias Scripta Met., 11,(1977),1101.

53. K.Tanaka and S.Matsuoka Int.J.Fracture,13,(1977),563.

54. F.A.McClintock and A.S.Argon "Mechanical behaviour of materials",Addison-Wesley, (1966), p.600.

55. R.O.Ritchie Met.Sci.,11,(1977),368.

56. J.Masounave and J-P.Bailon Scripta Met.,10,(1976),165.

57. M.Klesnil, M.Holzmann, P.Lukas and P.Rys JISI,203,(1965),47.

58. V.Weiss and D.N.Lal Met.Trans.,5,(1974),1946.

59. R.O.Ritchie Met.Sci.,11,(1977),368.

60. R.J.Cooke and C.J.Beevers Mat.Sci.Eng.,13,(1974),201.

61. R.J.Cooke, P.E.Irving, G.S.Booth and C.J.Beevers Eng. Fract.Mech.,7,(1975),69.

62. M.Klesnil and P.Lukas Mat.Sci.Eng.,9,(1972),231.

63. P.E.Irving and C.J.Beevers Mat.Sci.Eng.,14,(1974),229.

64. J.A.Feeney, J.C.McMillan and R.P.Wei Met.Trans.,1,(1970),1741.

65. M.F.Carlson and R.O.Ritchie Scripta Met.,11,(1977),1113.

66. E.K.Priddle Scripta Met.,12,(1978),49.

67. C.J.Beevers Met.Sci.,11,(1977),362.

68. R.J.Cooke and C.J.Beevers Eng.Fract.Mech.,5,(1973),1061.

69. R.A.Oriani and P.H.Josephic Acta Met.,22,(1974),1065.

70. G.T.Hahn and A.R.Rosenfield Trans.ASM.,59,(1966),909.

71. A.T.Santhanam Proc.2nd Int.Conf. on Mechanical behaviour of materials, Boston, (1976),1022.

72. S.Freeman Ph.D. thesis, University of Cambridge, 1971.

73. E.F.Walker and M.J.May BISRA Report MG/E/307/67.

74. J.R.Rice ASTM STP 415,(1967),247.

75. J.F.Knott Mat.Sci.Eng.,7,(1971),1.

76. H.Kitagawa, R.Yunki and T.Ohira Eng.Fract.Mech.,7,(1975),515.

77. C.J.McMahon Mat.Sci.Eng.,25,(1976),233.

78. C.J.McMahon "Grain boundaries in engineering materials", 4th Bolton Landing Conf., Baton Rouge, (1975),525.

79. C.Pichard, J.Rieu and C.Goux Mem.Sci.Rev.Met.,70,(1973),13.

80. J.R.Low, D.F.Stein, A.M.Turkalo and R.P.Laforce Trans. Met.Soc.AIME.,242,(1968),14.

81. M.Guttmann Surface Science,53,(1975),213.

82. E.D.Hondros, M.P.Seah and C.Lea Metals and Materials,(1976),26

83. L.A.Harris J.Appl.Phys.,39,(1968),1419.

84. H.Ohtani, H.C.Feng, C.J.McMahon and R.A.Mulford Met.Trans., 7A,(1976),87.

85. A.K.Cianelli, H.C.Feng, C.J.McMahon and A.H.Ucisik to be published.

86. C.L.Smith and J.R.Low Met.Trans.,5,(1974),279.

87. R.Viswanathan Met.Trans.,2,(1971),809.

88. J.M.Capus JISI.,200,(1962),922.

89. C.Ouchi, J.Tanaka and T.Osuka "Towards improved ductility and toughness", Conf. Kyoto, Japan (1971),67.

90. R.A.Mulford, C.J.McMahon, D.P.Pope and H.C.Feng Met.Trans., 7A,(1976),

91. P.E.Irving, M.P.Seah and A.Kurzfield Proc.2nd Int.Conf. on Mechanical behaviour of materials, Boston, ASM,(1976),563.

92. R.Viswanathan and T.P.Sherlock Met.Trans.,3,(1972),459.

93. R.A.Mulford, C.J.McMahon, D.P.Pope and H.C.Feng to be published in Met.Trans.

94. H.Ohtani and C.J.McMahon Acta Met.,23,(1975),377.

95. R.Narayan and M.C.Murphy JISI.,211,(1973),493.

96. C.J.McMahon, J.Yu, A.Yen and W.R.Graham Conf. Residuals, additives and materials properties, London, (1978).

97. P.Dumoulin and M.Guttmann to be published.

98. A.D.Batte, D.V.Edmonds and R.W.K.Honeycombe Proc. 2nd ICSMA, Asilomar, California, (1970),585.

99. S.Freeman ISI Special report No.145,(1971),152.

100. F.B.Pickering and T.Gladman ISI Special report No.81,(1963).

101. D.V.Edmonds and R.W.K.Honeycombe JISI,211,(1973),209.

102. R.B.Scarlin and J.W.Edington Met.Sci.J.,7,(1973),208.

103. D.Dulieu, D.J.Latham and P.Duhaj Proc. 2nd ICSMA, Asilomar, California,(1970),927.

104. G.L.Dunlop, D.V.Edmonds and R.W.K.Honeycombe Proc.Conf. on Creep strength in steel and high temperature alloys, (1972),222.

105. D.V.Edmonds, G.L.Dunlop and R.W.K.Honeycombe Proc.Conf. on Microstructure and design of alloys, Cambridge,(1973).

106. G.L.Dunlop Ph.D. thesis, University of Cambridge, 1974.

107. T.Gladman, I.D.McIvor and D.Dulieu Microalloying'75,25.

108. J.H.Smith and J.J.Vett Metal Progress,9,(1969),76.